MSc ANTHROPOLOGY
SCHOOL OF ANTHROPOLOGY AND CONSERVATION

Ontogenetic perspectives on modern human long bone growth: the humerus

---

Rosemary Jane Pitfield
2015

Supervisors: Dr. P. Mahoney and Dr. C.A. Deter

Abstract

Biological anthropologists routinely infer ancient human behaviour from macroscopic skeletal markers, although the underlying relationship between bone growth and functional adaptation remains complex. To date, few studies have undertaken a microstructural analysis of bone plasticity in relation to ontogeny. The primary aim of this study is to map histological changes within the humerus with age. If the histological changes have a strong correlation with age then it will be possible to produce a regression equation to predict juvenile age-at-death. This is the secondary aim of the study. The final aim is to ascertain how bone robusticity influences bone growth, within age-matched juveniles.

A sample of 83 juvenile skeletons from St. Gregory's Priory, Canterbury were aged using standard methods. One 0.5 cm histological section was removed from the anterior humeral midshaft of each skeleton. Histological slides were prepared using standard methods. The density and morphometrics of primary osteons and secondary osteons were recorded using a high resolution microscope.

Results show that primary osteon population density has a strong negative correlation with age (r_s = -0.672, N = 83, $p < 0.0005$). Secondary osteon population density has a strong positive correlation with age (r_s = 0.878, N = 83, $p < 0.0005$). A regression equation to estimate age at death from primary and secondary osteon population density was produced. The equation can be used to estimate juvenile age-at-death, between 0 - 17 years of age, with 86.1% accuracy. In an age matched sub-group robusticity was found to have a negative correlation with secondary osteon population density (r_s = -0.642, N = 35, $p < 0.001$).

Acknowledgements

First and foremost I would like to thank my supervisors Dr. P. Mahoney and Dr. C. Deter. Without their guidance and support throughout, this project would not have been possible. I would also like to thank Dr. J. Miszkiewicz for her help with the methodological design and techniques used in this project.

Additionally, I owe thanks to the School of Anthropology and Conservation at the University of Kent and the Skeletal Biology Research Centre for allowing access to the human skeletal remains.

CONTENTS

LIST OF TABLES

LIST OF FIGURES

GLOSSARY

The definitions of the terms that are defined in this glossary are all sourced from White et al., (2011) Human Osteology.

Directional Terms

- Sagittal plane: divides the body into symmetrical right and left halves.
- Coronal plane: divides the body into anterior and posterior halves.
- Transverse plane: divides the body perpendicular to the sagittal and coronal planes.
- Superior: toward the head of the hominid body.
- Inferior: opposite of superior, body parts away from the head.
- Anterior: toward the front of the hominid body.
- Posterior: opposite of anterior, towards the back of the hominid body.
- Medial: toward the midline.
- Lateral: opposite of medial, away from the midline.
- Proximal: nearest the axial skeleton, usually used for limb bones.
- Distal: opposite of proximal, farthest from the axial skeleton.

Movement Terms

- Flexion: a bending movement that decreases the angle between body parts.
- Extension: a straightening movement that increases the angle between body parts.
- Abduction: movement of a body part, usually a limb, away from the sagittal plane.
- Adduction: movement of a body part, usually a limb, toward the sagittal plane.
- Circumduction: a combination of abduction and adduction, as well as flexion and extension, that results in an appendage being moved in a cone-shaped path.

- Rotation: motion that occurs as one body part turns on an axis.
- Opposition: motion in which body parts are brought together.
- Pronation: rotary motion of the forearm that turns the palm from anteriorly facing to posteriorly facing.
- Supination: rotary motion of the forearm that returns the palm to facing anteriorly.

Bone Features

- Diaphysis: the long, straight section between the ends of a long bone.
- Epiphysis: the end portion of a long bone that is expanded for articulation.
- Articulation: an area where adjacent bones are in contact.
- Facet: a small articular surface on a bone.
- Head: a large, rounded, usually articular end of a bone.
- Condyle: a rounded articular process.
- Epicondyle: a non-articular projection adjacent to a condyle.
- Tuberosity: a large roughened eminence of variable shape.
- Tubercle: a small, usually roughened eminence, often the site of tendon or ligament attachment.
- Crest: a prominent, usually sharp and thin ridge of bone, often formed between adjacent muscle masses.
- Fossa: a depressed area, usually broad and shallow.
- Groove: a long pit or furrow.
- Foramen: an opening through a bone, usually a passage for blood vessels and nerves.
- Brachial: belonging to, or related to the arm.

CHAPTER 1.

INTRODUCTION

1.1 Introduction

The current understanding of human bone histology during ontogeny is extremely limited, compared to the histology of adult bone. Therefore, the primary aim of this project is to map how bone microstructure varies with age in a series of juvenile humeri. The robusticity of the juveniles is accounted for. Because this study will conduct the first comprehensive investigation of juvenile bone microstructure and age, it presents an opportunity to determine if age-at-death calculated for each juvenile corresponds with variation in bone microstructure. An estimation of age at death is an important part of a biological profile. However, the currently accepted methods of age estimation rely on the relative completeness of a skeleton. Many skeletal remains are incomplete. This is particularly true for the remains of juveniles. They have often been subject to different burial practices, accelerated decomposition compared to adults, and incomplete retrieval. It can be difficult to estimate age at death from current methods that rely upon complete skeletal components such as complete enamel crowns, intact long bones, or epiphyses. A histological method of age at death estimation would be of use in cases involving an incomplete skeleton. Consequently, the secondary aim of the study is to develop a method for predicting age at death from the bone histology.

This study will analyse the bone microstructure of 83 human juvenile humeri using standard histological methods. The juveniles studied range in age from neonates to

approximately 18 years of age at death. The skeletal remains are all from St. Gregory's Priory, Canterbury. The histological analysis will focus on the primary and secondary bone. This will allow a description of bone microstructural changes through ontogeny. The robusticity of the juveniles will be accounted for in the analyses of age and bone microstructure.

1.2 Aims

The primary aim of this study is to map bone microstructure through ontogeny. Bone tissue is dynamic and goes through several important changes throughout childhood and adolescence. The humerus begins developing as a cartilage model that is rapidly calcified to form a woven bone model. Overtime this woven bone is 'filled in' by primary lamellar bone with primary osteons. Osteons are tubular structural units within the bone that provide a more regular structure. As the bone grows in length and width more primary bone is deposited so that the diaphysis can expand. The diaphysis is the shaft of the long bone, which is shaped by cortical drift. Cortical drift is a part of this, in which the primary bone is remodelled and replaced by secondary bone in the form of secondary osteons. Gradually all of the primary bone will be replaced by secondary bone as strains in the bone lead to microcracks that need repairing. Histological methods can be used to quantify these changes in bone structure throughout ontogeny. For example, the densities of both primary and secondary osteons within the cortex can be calculated from histological methods. The density of secondary osteons is a proxy for the rate of remodelling in the bone (e.g., Streeter, 2012).

The secondary aim of this study is to determine if bone microstructure in juveniles can be use to estimate age-at-death. If any of the variables are found to have a significant strong correlation with age a regression equation can be produced from these variables. This regression equation could then be use to estimate juvenile age-at-death when the particular variables are entered into it. Potentially, the regression equation could be applied to a bone fragment. In these cases, a complete skeleton would not be required to estimate age-at-death.

The third aim of this study is to explore the relationship between bone robusticity and microstructure. It is important to account for the robusticity of the juveniles, in case this exerts an influence on the relationship between microstructural variables and age. However, this also presents a preliminary opportunity to explore aspects of inferred behaviour and bone morphology. In this study the sample will be split into three groups, one of more robust individuals, one of more gracile individuals, and an intermediate robusticity group that separates the two extremes. The aim is to determine if inferred behaviour corresponds with aspects of bone microstructure. It is possible to accomplish this because mechanical strains that are caused by activity cause the bone to be remodelled in response to strain. Although, the precise mechanism that causes this, termed mechanotransduction, is poorly understood at present (e.g., Martin et al., 1998). High levels of activity have been indicated as leading to more robust bone, and so it is likely that the most active children will have a higher robusticity index than less active children. As such robusticity of the humerus is used as a proxy for the level of activity an individual had during their lifetime.

1.3 Summary

Chapter 2 will be a review of the current literature that relates to the study. It will begin with an overview of the anatomy of the upper limb and a morphological summary of the humerus, including the musculature that is associated with it. Following this, the embryological development and subsequent growth of the humerus will be explained. This will cover the processes of endochondral ossification, intermembranous ossification, and periosteal apposition, as they apply to the humerus in particular. It will also explain the processes of modelling and remodelling during growth. The chapter will then explore how activity can affect bone microstructure through induced strains, and the competing theories that explain the mechanism responsible for this. This will lead into a description of primary and secondary bone microstructure, and an overview of the current methods for estimating age from bone histology. The chapter will conclude by situating the aims of this study within the context of the background literature.

Chapter 3 is the materials chapter. The chapter will describe the skeletal sample that was used in this study. It will list the selection criteria that were applied to the skeletal remains before they were included in the study, and why these criteria were important. Following this, there will be a description of the sample that satisfied the criteria, which will include a demographic breakdown of the sample. Next the archaeological background of the population that the sample was drawn from will be discussed.

Chapter 4 will explain the methodology that was used in this study. This will begin with the macroscopic methods followed by the microscopic methods. The macroscopic

methods were used to estimate age at death, and create robusticity indices for each skeleton. The microscopic methods section will have a step-by-step methodology for taking histological sections from bone, an overview of the principles of light microscopy, and the histological imaging technique from which the variables will be measured. The methods chapter will conclude by describing the ways in which the data will be analysed.

Chapter 5 will present the cover all of the results of the analyses which relate to the aims. Non-significant results will be included in tables in an appendix. The results chapter begins with descriptive statistics, which describe the distribution of the data. Inferential statistic results will make up the remainder of the chapter. These consist of the results of one way ANOVAs, Spearman's rho, Pearson's correlations, linear regression analysis, and multiple linear regression analysis.

Chapter 6 will discuss the results in relation to the study aims, and place them within the framework of current knowledge. The discussion of the results will follow the three aims of the study. Each will comprise an explanation of the results, and assessment of the results against each aim, and the current literature. The next part of this chapter will explain the limitations that have affected this study, and the steps that were taken to minimise these. The discussion chapter will finish with suggestions for future studies that will further the work of this study and assess its reliability.

Chapter 7 will conclude this study. It will summarise the main findings with reference to the three aims. It will also explore the implications of these results for the field of biological anthropology.

CHAPTER 2.

LITERATURE REVIEW

2.1 Introduction

This chapter introduces the anatomy and function of the upper limb, in particular the humerus. The embryological developmental phases and subsequent growth patterns of the humerus will be explained. This will include an explanation of the basic structure of bone followed by the functional properties of bone. The chapter will then cover the principles of histology that apply to the current project. The section finishes with an overview of the current histological ageing techniques.

2.2 Upper Limb Anatomy

Bones are part of the musculoskeletal system that protects and supports the soft tissues of the body. They provide an anchor for the muscles, tendons, and ligaments, which produce bodily movements (Grey, 2012). In humans, the upper limb is made up of several elements that cooperate to produce both large movements of the arm and fine movements of the hand. The upper arm bone is the humerus, which articulates with the scapula at the shoulder, and with the radius and ulna at the elbow. It is the largest bone in the upper limb (White et al., 2011). The radius and ulna articulate with the scaphoid and lunate at the wrist (White et al., 2011). The hand contains twenty-seven bones, eight

are carpals, five are metacarpals, and fourteen are phalanges. The complexity of the hands skeletal structure affords it an enormous range of movement, including fine motor control such as pinching and pointing.

2.3 Humeral Morphology

The humerus is one of the major long bones in the body. The major function of these type of bones is movement. In order to produce movement, the humerus is associated with a complex musculature, especially due to its varied use. The human arm is capable of circumduction, as well as flexion, extension, and pronation and supination of the forearm (White et al., 2011). As such the humerus has a complicated pattern of loading that influences its morphology, particularly during ontogeny. The major morphological features of the humerus are shown in **Fig. 2.1**.

The proximal humerus has a spherical head that articulates with the glenoid fossa of the scapula (White et al., 2011). The rounded articular surface permits free movement in the joint, which allows the arm to move in most directions at the shoulder. This type of arm swinging motion is known as brachiation. Lateral to the head are the greater and lesser tubercles of the humerus. These provide the attachment sites for the supraspinatus, infraspinatus, teres minor, and subscapularis muscles. Together these are known as the rotator cuff muscles, which are responsible for the rotation of the arm and aid in the abduction and adduction of the arm. They are also responsible for holding the humeral head against the glenoid fossa and stabilising the joint (White et al, 2011).

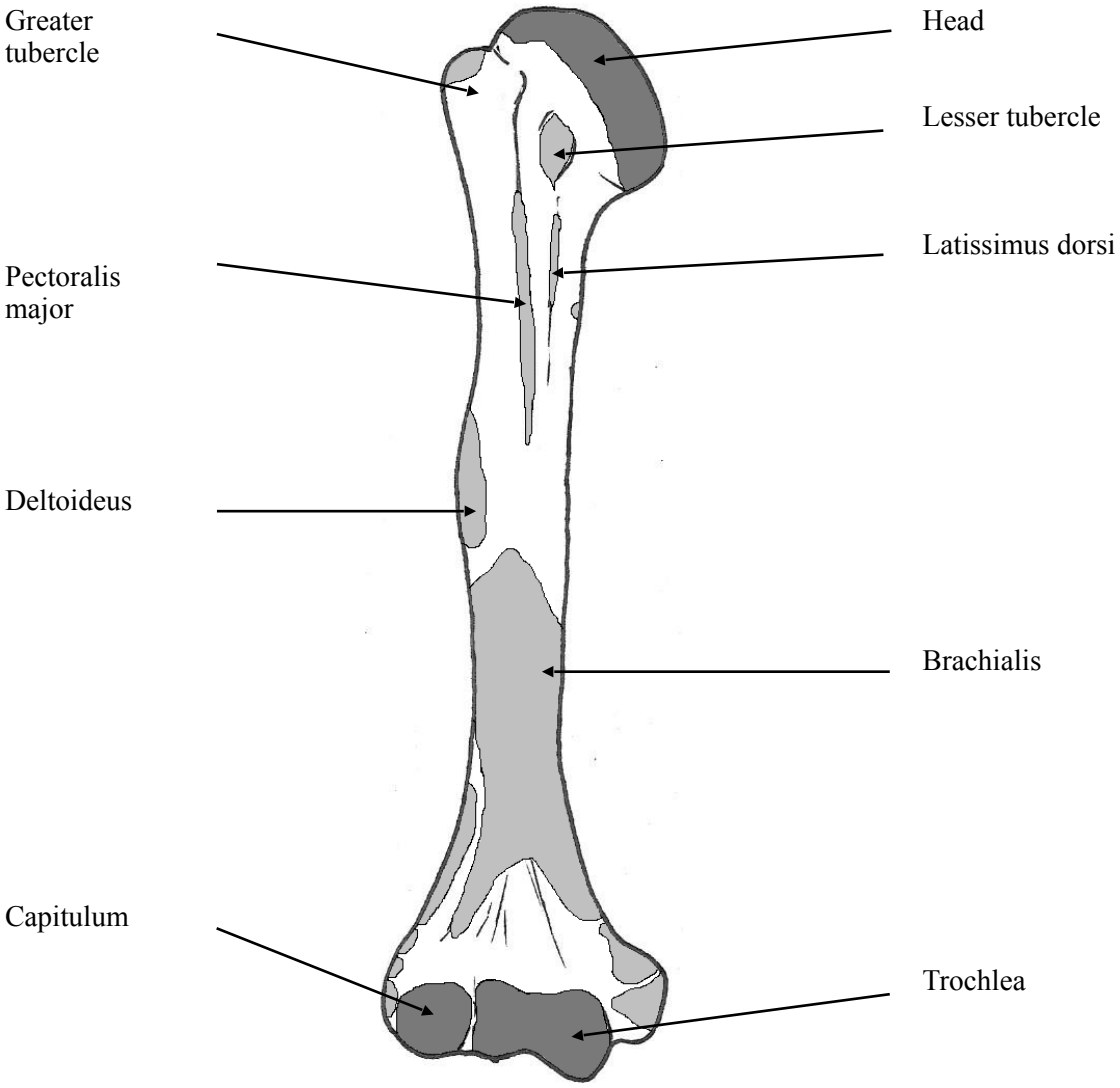

Fig. 2.1 The humerus morphology and musculature, annotated with the major features. Light grey = Muscle attachment site. Dark grey = articular surface.

The shaft of the humerus is quite rounded proximally, but more triangular distally in cross section (White et al., 2011). It has three surfaces that can be distinguished; the anteromedial surface, the anterolateral surface, and the posterior surface. Between the tubercles is the intertubercular sulcus which continues distally onto the anteromedial surface as the bicipital groove. This is bordered by the crest of the greater tubercle laterally and the crest of the lesser tubercle medially. The pectoralis major muscle flexes, adducts and medially rotates the arm, and has an insertion on the greater crest.

The insertion site latissimus dorsi and teres major muscles are located on the lesser crest. These muscles adduct and medially rotate the arm (White et al., 2011). The deltoid tuberosity is located on the anterolateral surface around the midshaft. This area is slightly elevated and roughened, which marks the insertion site for the deltoideus muscle, the main abductor of the arm. Below the midshaft both the anteromedial surface and the anterolateral surface are covered by the muscular origin of the brachialis, while the posterior surface below the midshaft is covered by the muscular origin of the triceps brachii (White et al, 2011). These muscles are the primary flexors and extensors of the forearm respectively. They are the main muscles responsible for movement at the elbow. The brachioradialis originates on the lateral border between the anterior and posterior surfaces and assists with the flexion of the forearm.

The distal humerus articulates with the radius and the ulna of the forearm at the elbow joint (White et al., 2011). The capitulum is a rounded eminence on the lateral side of the epiphysis, which articulates with the radial head. Next to the capitulum on the medial side is the trochlea, which articulates with the ulna notch (White et al., 2011). On the posterior side of the distal epiphysis is the large olecranon fossa that receives the olecranon process of the ulna when the forearm is fully extended. On either side of the humeral distal articular facets are the medial and lateral epicondyles (White et al., 2011). The medial epicondyle is more prominent than the lateral epicondyle, and has attachment sites for muscles that pronate the forearm, and flex the wrists and fingers. The lateral epicondyle has attachment sites for the extensor muscles of the wrists and fingers (White et al, 2011).

2.4 Humeral Development

The development of the humerus begins in utero and can be seen as limb buds in the embryo. An embryo is an unborn child at less than 8 weeks gestation. After 8 weeks gestation it is known as a foetus. The upper limb buds can be recognised as slight elevations at around the 26th day of gestation (O'Rahilly and Gardner, 1975). After 32 days the buds have formed rounded projections that curve ventrally and medially, and taper towards the end. The hand plate, a flattened expansion at the end of the limb, becomes recognisable by the 33rd day (O'Rahilly et al., 1956). The internal mesenchymal condensations for the humerus, radius, and ulna are formed by the 37th day. The mesenchymal condensations are a network of primitive connective tissue from which all other connective tissue will be formed, including bone and cartilage. They are the precursors of the cartilage models, which themselves are the precursors of the ossified bones. The mesenchyme condenses to a pre-cartilage blastema (Hamilton et al., 1972). The blastema contains pluripotent cells that will later differentiate into cartilage cells (Tsonis, 2008). Each cell within the blastema secretes a basophilic matrix, which is a permeable ground substance that contains many collagen fibrils as well as chondrotin sulphate (Scheuer and Black, 2000). This stimulates the differentiation of mesenchymal cells into chondroblasts. Differentiation is the process in which cells change from one type of cell to another more specialised type of cell (Slack, 2012). As the blastema develops, an increase in the enzyme hyaluronidase causes the level of hyaluron to fall. Hyaluron is a type of polysaccharide called a glycosaminoglycan (Fraser et al., 1997). It is responsible for inhibiting chondrogenesis. Its reduction marks the beginning of cartilage model formation (Knudson and Toole, 1987).

As the cells continue to differentiate, early hyaline cartilage is formed. Chondrification is the process in which cartilage is formed from condensed mesenchyme tissue (Scheuer and Black, 2000). The cells at the edge of the blastema condense into a bilaminar perichondrium. This is a dense membrane that surrounds elastic cartilage and hyaline cartilage. Neither fibrocartilage or articular cartilage have a perichondrium. Chondroblasts line the inner layer of the perichondrium, which will be responsible for the later appositional growth of the cartilage (Glenister, 1976). The cartilage grows by way of cell division into a model of the bone that will later replace it (Scheuer and Black, 2000).

2.5 Humeral Endochondrial Ossification

Endochondrial ossification is a process by which a hyaline cartilage model is gradually replaced by a hard mineral, calcium hydroxyapatite ($Ca_{10}[PO_4]_6[OH_2]$) in order to form bone (Scheuer and Black, 2000). Endochondrial ossification can be divided into five phases, illustrated in **Fig 2.2**.

PHASE 1. Cartilaginous models begin to form at the start of gestation and are complete before 56 days gestation. Cells at the edge of the blastema condense to produce a bilaminar perichondrium. This is a thin membrane that will surround the cartilage model and which becomes the periosteal membrane. The inner layer of this is lined with cartilage forming chondroblasts that secrete the matrix of the cartilage. Chondrofication of the humerus begins with the shaft, followed by the head and epicondyles. The neck,

tubercles, and condyles form last. This marks the first stage in the process of endrochondral ossification (Scheuer and Black, 2000).

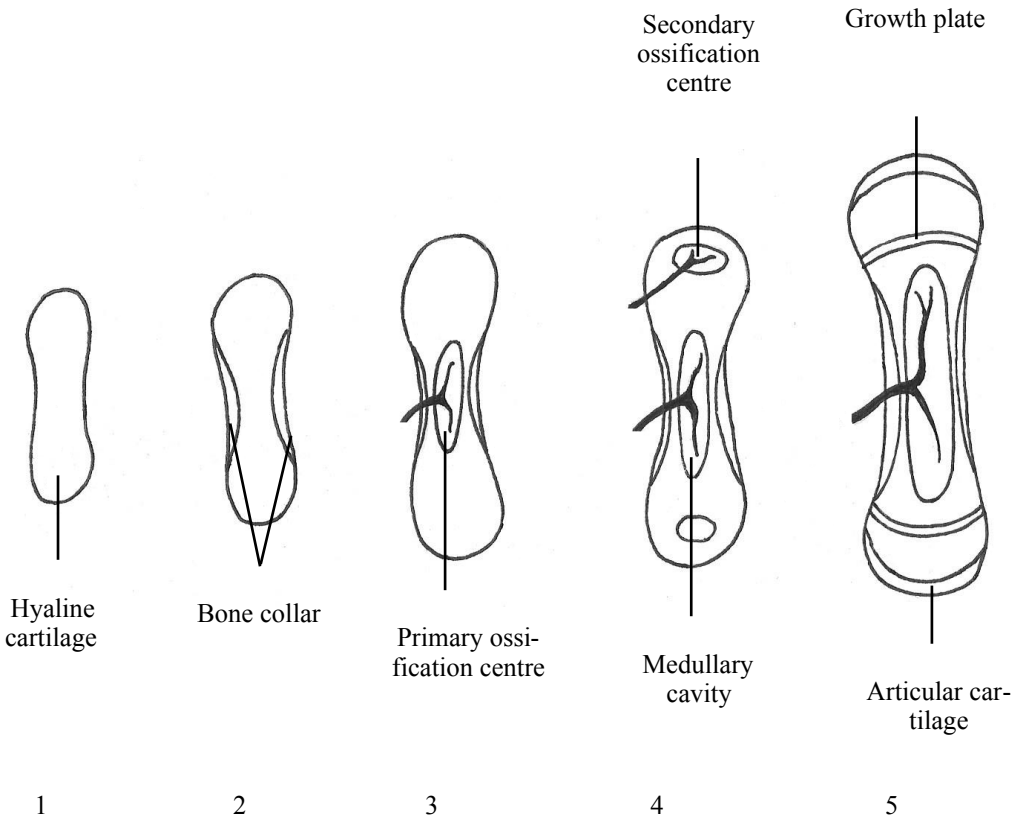

Fig. 2.2 Endochondrial ossification, stages 1 to 5.

PHASE 2. The perichondrium becomes the periosteum, which encases all bone that is not covered by articular cartilage. It is a vascular membrane that provides nourishment to the bone that it covers (Scheuer and Black, 2000). The membrane is lined with bone forming osteoblast cells that are retained throughout life (Shopfner, 1966). A bony collar develops around the perimeter of the cartilage diaphysis. This is caused by osteoblasts secreting an organic bone matrix called osteoid. Osteoid is composed of type 1 collagen and ground substance containing chondroitin sulfate and osteocalcin (Martin et al., 1998; Marks and Odgren, 2002; Robey and Boskey, 2009). Inorganic calcium phosphate in the form of hydroxyapatite is then secreted into the osteoid to calcify the

organic bone matrix. Mineralisation of the matrix occurs when the osteoblasts extrude vesicles containing alkaline phosphatase. This cleaves the phosphate group from the hydroxyapatite molecule, and allows calcium and phosphate to be deposited (Anderson and Morris, 1993; Scheuer and Black, 2000). Mineralisation happens due to an interaction between calcium binding molecules and the alkaline phosphatase. This first bone type is immature woven bone, which is coarse and contains non-oriented collagen fibrils but it is formed quickly. It is temporary, and is soon replaced by primary bone.

PHASE 3. In the third phase of endochondral ossification a nutrient foramen forms in the cortical bone of the diaphysis (Scheuer and Black, 2000). This transmits blood vessels to the interior so that the blood supplies osteoblasts to enter the centre of the cartilage model. 88% of people have a single artery located in the midshaft region, but more than one can exist (Skawina and Wyczolkowski, 1987). Here, the osteoblasts begin to form trabecular bone at the site of the primary ossification centre. Trabecular bone differs from cortical bone in several key ways. Trabecular bone is composed of many thin spicules of bone called trabeculae. As such, it is more porous, lightweight and spongy in appearance than cortical bone. It also houses red bone marrow, which is the site of haematopoiesis (Bruder and Caplan, 1989). This is the production of the blood products, including red blood cells, white blood cells, and platelets. Its structure provides higher tensile strength, and so it is found in the epiphyses and under muscle attachments which must resist higher mechanical forces than the diaphysis. However, the molecular composition of the two bone types is identical and they are both made of lamellar bone (Scheuer and Black, 2000).

PHASE 4. During the fourth phase, the newly laid trabeculae within the diaphyses are absorbed by osteoclasts and the red bone marrow is replaced by yellow bone marrow. This creates a medullary cavity containing yellow bone marrow, which acts as a fat reserve for the body. The medullary cavity is encased in the cortical bone, which replaced the woven bone of the bony collar. Cortical bone has a much more regular arrangement than either trabecular bone or woven bone (Crowder and Stout, 2012). It is composed of orderly tubular units called osteons, which are also known as Haversian systems. These are made up of concentric rings of lamellar bone around a central Haversian canal. They constitute the basic structural unit (BSU) of compact bone. The border between the cortical bone and the medullary cavity is lined with another vascular membrane, called the endosteum. Both the endosteum and the periosteum are osteogenic tissues that are lined with bone forming osteoblasts. These are numerous in juveniles when there are intense periods of prolonged bone growth, but reduced in number in adults who have completed bone development. However, the osteogenic potential is retained throughout life (Scheuer and Black, 2000).

This fourth phase also marks the appearance of secondary ossification centres. Ossification of the humerus is complex and involves multiple ossification centres. The primary ossification centre is located in the region of the mid shaft of the diaphysis (White et al., 2011). Additionally, there are three secondary ossification centres in the proximal epiphysis, the head and the greater and lesser tubercles, and four secondary ossification centres in the distal epiphysis, the capitulum, medial epicondyle, trochlea, and lateral epicondyle. The two groups of secondary ossification centres will eventually fuse to one another, giving rise to a proximal and distal compound epiphysis (Scheuer and Black, 2000).

PHASE 5. The final phase involves the formation of diaphyseal growth plates between the diaphysis and the epiphyses, as shown in Fig 2.3. As the bone growth at the primary ossification centre approaches that of the secondary ossification centres a band of cartilage remains which separates the regions (Rang, 1969). At the epiphyseal side there is a terminal plate. This separates the diaphysis from the epiphyses. The cartilage band contains four differentiated layers: the germinal zone, the proliferating zone, the degenerating zone, and the ossification zone. These zones are responsible for both the longitudinal growth and the diametric expansion of the bone (Scheuer and Black, 2000).

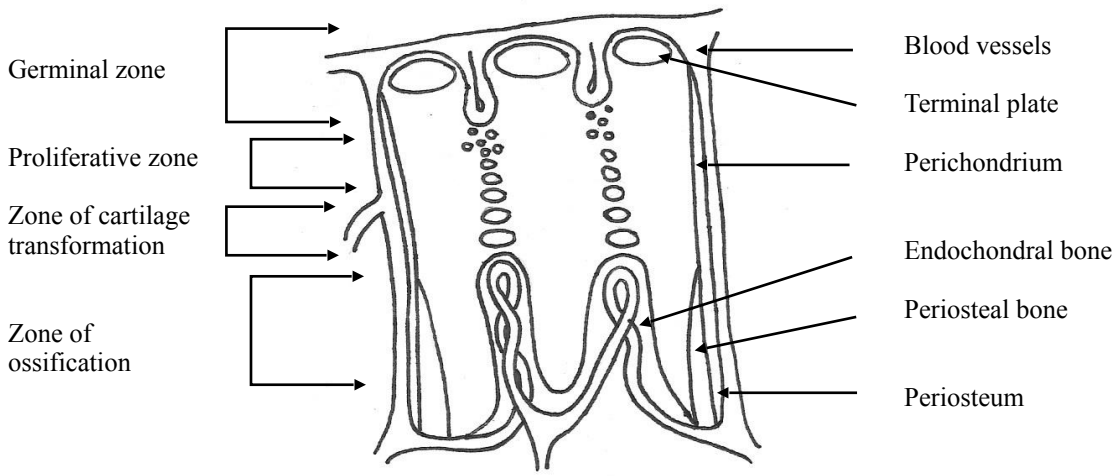

Fig. 2.3 Growth plate separating the diaphysis and epiphysis in a long bone.

The germinal zone is furthest from the diaphysis and contains randomly located quiescent chondrocytes. It receives a vascular supply from nearby epiphyseal blood vessels which penetrate the terminal plate. The next zone is the proliferating zone in which the chondrocytes accumulate glycogen and grow larger. In this zone, the cells are organised into pillars that can make up to half of the height of the growth plate. The chondrocytes begin to hypertrophy in the degenerating zone, ready to be replaced by bone cells, although some of the cells may travel to the next zone to become osteoblasts. At this point, hydroxyapatite crystals are being deposited by matrix vesicles to

mineralise the cartilage. In the ossification zone, closest to the diaphysis, a layer of bone is deposited onto the mineralised cartilage of the preceding zone by osteoblasts. Osteoclasts reorganise this new bone so that it is more regular and organised than the originally deposited bone. When the rate of bone formation, osteogenesis, surpasses the rate of cartilage formation, chondrogenesis, the process of epiphyseal fusion commences. This is when the cartilage band decreases in size and the bones of the diaphysis and epiphyses come together and fuse (Scheuer and Black, 2000).

In addition to the diaphyseal growth in length, the epiphyses increase in size via spherical growth plates. These growth plates are similar to those of the shaft. There is a proliferating zone in which cartilage cells are produced. These cells are progressively replaced by immature woven bone by the centrifugal expansion of endochondral ossification (Ogden et al., 1979). As the secondary ossification centres expand they will fuse with one another, and will eventually approximate with the growth plate of the diaphysis. When the bone formation in the epiphysis reaches this location, the terminal plate is produced by the trabeculae uniting to seal the epiphysis from the diaphysis (Weinmann and Sicher, 1947). This also ensures that the red marrow of the epiphysis is kept separate from the yellow marrow of the diaphysis.

Once the growth plates have closed the bone cannot increase in length (Scheuer and Black, 2000). The order and timing of the fusion of the epiphyses is usually constant. As such epiphyseal closure is commonly used to assign an age to a set of juvenile skeletal remains (McKern and Stewart, 1957). The humeral growth plates are some of the earliest to appear, but among the latest to close. At the proximal epiphysis of the humerus, the secondary ossification centre for the head usually appears at

approximately six months postpartum, although it can be formed by birth (Spencer, 1891; Davies and Parsons, 1927; Menees and Holly, 1932). Next to form is the secondary ossification centre for the greater tubercle at some point between three months postpartum and three years (Elgenmark, 1946; Hansman, 1962; Garn et al., 1967). The third and final ossification centre of the proximal epiphysis is for the lesser tubercle, which appears between four and five years (Cocchi, 1950). However, the presence of the third centre is contentious; some researchers believe that it does not exist (Cohn, 1924; Paterson, 1929; Ogden et al., 1978; Caffey, 1993). The three centres coalesce to form a compound epiphysis at between five and seven years, but the fusion is not complete until approximately seven to eight years (Scheuer and Black, 2000). It is the proximal end of the humerus that is responsible for the majority of the growth in shaft length; about 80% of the total growth occurs at the proximal end (Ozonoff, 1979; Ogden, 1984d; Pritchett, 1991). Consequently, it has one of the slowest fusing epiphyseal plates, as more time is needed to obtain the full length of the bone as the body grows throughout adolescence. The ossification centres of the proximal and distal humerus are shown in **Fig 2.4**.

Fusion to the shaft commences from the posterior region between the head and greater tubercle, at approximately 15 to 18 years. The junction of the anatomical and the surgical necks at the anterior region of the bone fuses next, and the fusion then progresses medially (Haines et al., 1967). This results in the head and shaft becoming attached, while the epiphyseal plate underneath the greater and lesser tubercles remains open. Following this, fusion occurs at the sulcus between the tubercles, from the lateral lip towards the lesser tubercle. The area beneath the greater tubercle is the last to fuse to the diaphysis. Although, Ogden et al. (1978) believe that this pattern can vary between

individuals. The fusion of the proximal epiphysis is usually fully complete between 16 years and 22 years (McKern and Stewart, 1957).

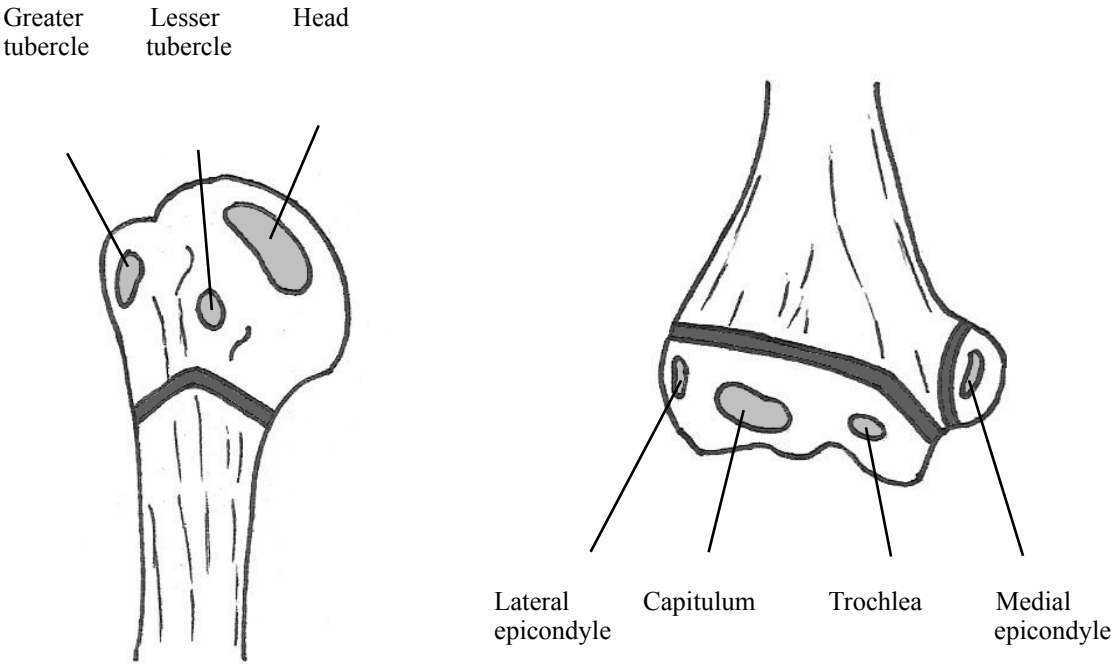

Fig. 2.4 Secondary centres of ossification of the proximal and distal humerus.

At the distal end of the diaphysis the first of the four secondary ossification centres is for the capitulum, which can appear at six months postpartum but is usually present by two years (Silberstein et al., 1979). The next centre, which can be seen at around four years, is for the medial epicondyle (Silberstein et al., 1981). The trochlear ossification centre develops at approximately eight years and quickly fuses with the capitulum along its lateral edge. Finally, the lateral epicondyle becomes visible around the age of ten and its distal part soon fuses to the lateral edge of the capitulum (Silberstein et al., 1982). This results in a compound epiphysis with a separate medial epicondyle by ten years in females and 12 years in males (Haraldsson, 1959).

Diaphyseal fusion begins in the posterior portion of the epiphyseal plate soon after the compound epiphysis has formed, and is usually complete by 15 years in females and 17 years in males. The medial epicondyle is the last part of the distal epiphysis to fuse to any other element. It fuses first on the inferior edge at 13 to 15 years in females and 14 to 16 years in males (Paterson, 1929). The anterior and superior regions are the last to fuse, at around 15 to 17 years in females and 16 to 20 years in males (Hansman, 1962).

2.6 Bone Growth

Growth is a general term that encompasses the incremental increase in size and morphology of a tissue throughout the developmental period of an individual (White et al., 2011). It can pertain to both an increase in size and an increase in maturity, which do not necessarily happen together. Due to this, different individuals will obtain particular developmental stages, or biological age, at different chronological ages. Growth in length is caused by bone formation at the growth plates, but alongside this, there is also diaphyseal expansion by way of periosteal intramembranous ossification. This is required because longitudinal growth cannot result in the correct morphology on its own.

Intermembranous ossification is the mineralisation of the periosteal membrane (Scheuer and Black, 2000). This process is responsible for the mineralisation of the flat bones in the body, such as the skull and clavicle. It is also responsible for the outward expansion of the diaphysis via appositional growth (Enlow, 1963; Garn, 1970; Martin et al., 1998). The diameter of the shaft increases as osteoblasts deposit layers of lamellar bone onto

the external surface of the shaft. At the same time, osteoclasts remove bone from the endosteal surface that lines the medullary cavity. Eventually, this process replaces all of the original woven bone with primary lamellar bone and an enlarged medullary cavity.

Additionally, the curvature of the long bones can be adjusted during appositional growth by increasing the deposition and resorption on the sides of the bone so that its cross section moves sideways relative to the epiphyses. This is known as cortical drift (Martin et al., 1998). During the lateral drift of a diaphysis, new bone lamellae must form on the medial surface of the endosteum while those on the lateral endosteal surface must be resorbed. Concurrently, lamellae must form on the lateral surface of the periosteum while one on the medial periosteal surface is resorbed. This is the only way that the medullary cavity can remain within the centre of the drifting diaphysis. The cross section of the diaphysis changes in thickness and shape asymmetrically during growth (e.g., Ruff, 2000; McFarlin, 2006; Goldman et al., 2009; Maggiano, 2011; Gosman et al., 2013).

Bones are made up of living tissues, which is why they can undergo growth, remodelling and repair. Bone tissue is continuously broken down and then replaced as the bones grow, and then maintain their shape, and reorganise in response to mechanical stress. There are three types of cell that largely responsible for the formation and maintenance of bone tissue: osteoblasts, osteocytes, and osteoclasts. Osteoblasts are bone forming cells, that have differentiated from osteoprogenitor cells (Martin et al., 1998). They secrete the organic component of bone, osteoid, and promote the deposition of inorganic crystals, such as calcium and phosphate, into the bone matrix. Some of these cells will become bone lining cells on the surfaces of the bone, and control the

release of calcium into the blood in response to changing hormone levels. Osteocytes are mature cells that have differentiated from osteoblasts, and become encased in bone (Martin et al., 1998). They work to maintain the structure of the bone tissue. Osteoclasts are bone resorbing cells, formed by the fusion of several monocytes (Martin et al., 1998). They break down the bones structure by demineralising the mineral portion of the bone with acid and then dissolving the collagen with enzymes. This releases the inorganic mineral components into the blood which is important for homeostasis, the stable condition of the body.

All of primary bone growth is encompassed by the term modelling. In the long bones it involves the increase in length and width, the reduction of the metaphyses, and cortical drift. Together, all of these processes lead to the attainment of a bones proper size and morphology (Cambra-Moo et al., 2014). Modelling is when new bone is laid down at a site that has never been bone tissue. As such osteoclasts are not present as there is no old bone to remove. Modelling is the result of the sole action of osteoblasts.

The osteoblasts and osteoclasts remain active throughout life, albeit at a much slower rate. Remodelling begins in the first few months of life (Burton et al. 1989) and there is continuous remodelling of the bone over the whole lifespan. Remodelling differs from modelling because it is the process in which old bone is replaced by new bone by the linked action of osteoclasts and osteoblasts. During remodelling the bone deposition by osteoblasts is balanced by the bone absorption by osteoclasts, so the overall size and shape of the bone remains the same. Approximately 5% of adult cortical bone and 25% of adult trabecular bone in replaced every year (Martin et al., 1998). As the body ages

the remodelling process slows down and bone absorption may overtake bone deposition, leading to a reduced bone density, known as osteoporosis.

Remodelling is based on the action of basic multicellular units (BMUs) of remodelling, which are composed of osteoclasts and osteoblasts. The product of the BMU is a basic structural unit (BSU), also known as a secondary osteon or a Haversian system (Martin et al., 1998). It occurs throughout the bone, but is most easily seen within the cortical bone. Remodelling has three stages: activation, resorption, and formation.

STAGE 1. The process begins with the activation phase, in which osteoclasts appear at the site that is to be remodelled. They are called to that point in response to osteocytes, in lacunae, that have sensed systemic and biomechanical changes. Some bone is resorbed by osteoclasts which leaves a cavity, known as either a resorptive bay or cutting cone when in cortical bone (Parfitt, 2005). The BMU's resorption follows the trajectory of the mechanical strain that was previously sensed. Most commonly in long bones this is longitudinally (van Oers et al., 2008). The diameter of the cutting cone is usually between 150 and 350μm, which dictates the diameter of the osteon that BMU will later form to fill the void (van Oers et al., 2008).

STAGE 2. Immediately behind the advancing cutting cone is a new capillary, which nourishes the BMU and allows osteoclast precursor cells to reach the BMU. In a brief reversal phase that happens between the resorptive and formative phases mononuclear cells line the cutting cone. It is not currently clear what the functions of these cells are, but it is suggested that they smooth off the scalloped edge of the cutting cone. This is to prepare it for a thin mineral-deficient, sulphur-rich layer of matrix to be deposited onto

it. The layer is called a reversal line and it separates a BSU from surrounding interstitial lamellar (Everts et al., 2002; Robling et al., 2006).

STAGE 3. After the reversal phase, the osteoblasts in the BMU secrete an osteoid. An osteoid is a substance that is composed of type 1 collagen and other non-collagenous proteins, proteoglycans, and water (Martin et al., 1998; Marks and Odgren, 2002). Calcium phosphate crystals are deposited into the osteoid to mineralise it. However, there is a lag time of approximately ten days between when the osteoid is deposited and when it is mineralised (Martin et al., 1998) so a layer of osteoid can be found between the osteoblasts and the mineralised bone.

Osteoclasts always undergo apoptosis after they have finished resorbing bone. However, one of three things will happen to an osteoblast. Some do undergo apoptosis like the osteoclasts, but others will become trapped within the matrix that they secreted and differentiate into osteocytes. The rest of the osteoblasts will differentiate into flat bone lining cells, which line the bone surface (Everts et al., 2002). Both the osteocytes and the bone lining cells are important generally for bone metabolism and particularly for bone remodelling. The embedded osteocytes produce cytoplasmic processes that extend within small channels, called canaliculi. These allow the osteocytes to communicate with surrounding cells via gap junctions. It is now thought that the major role of osteocytes is biomechanical, because they sense mechanical strains within the bone and initiate the micro-fracture repair process. Osteocytes continuously send signals that inhibit the activation of new BMUs, and when this signal is disrupted by osteocyte apoptosis or bone micro-fracture a new modelling cycle is activated (Martin, 2000).

2.7 Remodelling Theories

There are several theories that seek to explain how and why bone modelling and remodelling occurs, including Wolff's law, the mechanostat theory and the optimisation theory. Wolff's law is composed of three concepts: bone is formed and resorbed to maintain a balance between weight and strength, trabeculae within cancellous bone align along the axis of principle stress, and both processes are self regulated in response to mechanical strain (Martin et al., 1998). Originally Wolff's law was formulated to explain the trabecular orientation in the proximal femur (Wolff, 1892) but over time it became a more generalised principle of bone organisation and formation (Pearson and Lieberman, 2004). In its strictest sense it does not apply to diaphyseal cortical bone.

The mechanostat hypothesis explains that strains above a particular threshold will stimulate bone growth but inhibit Haversian remodelling, while strains below a lower threshold will inhibit growth and stimulate Haversian remodelling (Frost, 1986, 1987, 1990). Strains that are between the two thresholds will not stimulate either modelling or remodelling. However, few studies completely support this hypothesis. While high strains often cause bone modelling and low strains are correlated with bone resorption (Martin et al., 1998) high strains have also been found to stimulate bone remodelling (Goodship and Cunningham, 2001; Lieberman et al., 2003). Furthermore, the mechanostat hypothesis does not account for the variation in the bony response to loading in different bones across the skeleton, and between ontogenetic stages (Pearson and Lieberman, 2004).

Optimisation theory predicts how different bones in the skeleton respond to loading (Lieberman and Crompton, 1998; Lieberman et al., 2001; Lieberman et al., 2003). Specifically, it predicts that if bones optimise strength relative to the cost of growing new bone, and if remodelling repairs microcracks, then the proportion of modelling versus remodelling in response to loading will vary across the skeleton and at different ages in relation to their cost/benefit ratio (Pearson and Lieberman, 2004). The most important benefit of modelling is that the added mass will increase the strength of the bone, which is particularly important in response to bending. However, the cost of adding mass to the limbs is that the energy needed to propel the limb during locomotion will be higher (Marsh et al., 2004). The cost is higher in more distal parts than more proximal parts, as these regions require more energy. The costs and benefits of remodelling are less well known, but the benefits may include the replacement of damaged and fatigued bone, an increase in elasticity, and reduced micro-crack propagation (Martin et al., 1998; Schaffler et al., 1990; Currey, 2002). A known cost of remodelling is a higher long-term metabolic cost because further remodelling will be required in the future (Martin, 1995). The modelling response to strains declines with age and the bones, so the rate of remodelling increases in proportion to the strain in order to repair or limit fatigue damage (Lieberman et al., 2003).

At present it is not clear which theory best explains bone remodelling in response to strain. None of the current theories can fully explain bone growth and remodelling. Further histological data may help to support one of the current theories or it may lead to the formation of a new theory. It is possible to examine bone modelling and remodelling by using bone histology. The relative quantities of primary and secondary bone types within a bone can be used as a proxy for the level of remodelling in that

bone. As such archaeological bone studies can be useful because the histological features can be directly viewed. Whereas in a longitudinal living study examining the bone microstructure is difficult.

2.8 Biomechanics

In recent years there has been a vast increase in knowledge of skeletal growth and biomechanics. More is now known about the cells that control bone growth and maintenance; as well as about how bones sense and respond to mechanical strains. Bones adapt to their environment over time, but cortical bone responds most to loading during the juvenile period (Pearson and Lieberman, 2004). There are many forces that act upon bone. The bones have to respond to the forces by adapting their structure. If they did not respond it would leave them vulnerable to fatigue and fracture.

Two of the most important forces that affect bones are stress (σ, defined as force, F, per unit area, A) and strain (defined as change in length, ΔL, per unit length, L). Stress is the load per area and strain is the fractional change in dimension of a loaded body (Martin et al., 1998). The forces imposed on the bone generate stresses of variable intensities, which cause strains of variable magnitude (Pearson and Lieberman, 2004). The strain can be either tensile or compressive, but are usually a combination of the two, with the ratio depending on the type and intensity of mechanical loading. The loading typically occurs in four ways (**Fig 2.5**), axial compression, bending, shearing, and twisting (Carter and Beaupré, 2001).

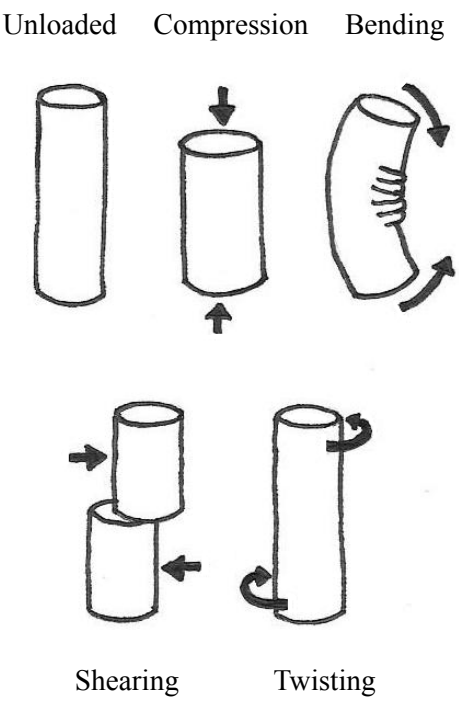

Fig. 2.5 Loading conditions that can affect the humerus.

Due to bone being composed of both cartilage and nonorganic mineralised tissue, it has a high degree of both strength and stiffness in response to mechanical forces. When low loads are applied to the bone it responds elastically as the bone regains its original form when the load is removed. However, above a particular threshold, called the yield point, bone responds plastically and permanently deforms up to the point at which it fractures (Pearson and Lieberman, 2004). The mechanical properties of bone are affected by many intrinsic and extrinsic factors. Some intrinsic factors are the amount of mineralisation, and the organisation of the tissue, including the histological structure, porosity, and collagen fibre orientation (Martin et al., 1998). The extrinsic factors include the mode, duration, and rate of the strains (Pearson and Lieberman, 2004).

When the skeletal muscles contract, mechanical stress is transmitted to the bone. Hence muscle use is directly responsible for the strain induced modelling and remodelling.

Muscles and tendons are crucial for proper bone function. When muscles contract the tendons transmit the tensile load to the bone surface, resulting in joint motion and posture maintenance. The bone acts as a pulley mechanism when tendons transmit forces around corners to distance muscle bellies from the joints (Currey, 2002; Benjamin et al., 2003). Together, the muscles and tendons are known as muscle-tendon units, which respond to dynamic loading. They can also repair after they are damaged, and respond to variable loading through tensile strength modifications (Bloebaum and Kopp, 2004). This is similar to bone modelling and remodelling due to microdamage and loading.

Tendons are composed of fibroblasts that are surrounded by extracellular matrix. Approximately 80% of connective tissue is composed of extracellular matrix, which itself is around 70% water and 30% collagen, ground substance and elastin. The fibroblasts that are found in tendons are arranged in longitudinal rows that are separated by collagen fibres and other organic minerals (Benjamin and Ralphs, 1998). They communicate with one another via gap junctions, which may be how tendons detect and respond to strain (Schlecht, 2012). The collagen is arranged in fibrils, which collectively form collagen fibres. The collagen fibres give the tendon strength and flexibility, as collagen has the highest tensile strength of any soft tissue. Bundles of collagen fibres are called fascicles. These are ensheathed in a loose sheet of connective tissue called endotenon. Finally, the fascicles unify to form the tendon, which is also ensheathed in connective tissue, the epitenon (Schlecht, 2012). The sheaths of connective tissue are important for reducing friction when the fascicles and tendons slide past one another. This possibly reduces the chance of failure and allows the structural adaption to compression and shearing.

Tendons and bones have a similarly high tensile strength (Thomopoulos et al., 2011) but tendons have a much lower compressive strength than bones. It is this variability in the material properties of tendon and bone that makes a complex enthesis necessary when connecting tendon to bone. The enthesis marks the point where tendon joins to bone, and mechanical stress is concentrated here (Benjamin et al., 2002). Opposing elastic fibres balance the tensile loads and dissipate the stress away from the osteotendinous junction and into the adjoining materials. As well as the transmission of forces, entheses provide an anchor to tendons, which enables tendons to resist the loads imposed upon them by the muscles. At the enthesis, the tendon fibres splay to form a firmly anchoring plexus. Some insertion sites overlap each other to gain greater tendon security.

Muscle insertion sites are areas where muscles and tendons are anchored to bone. Entheses can be either fibrous or fibrocartilaginous depending on what type of tissue is present and where it is located on the bone. Fibrous entheses attach along long bone diaphyses, whereas fibrocartilaginous entheses are only found on long bone epiphyses. This distinction is caused by the differing origin of the different regions of the bone; the diaphysis ossifies by intramembranous ossification and the epiphysis ossifies by endochondral ossification. Fibrous entheses are rooted in thick layers of cortical bone and ossify intramembranously, while fibrocartliaginous entheses are rooted in thin layers of cortical bone and ossify endochondrally (Schlecht, 2012).

Damage occurs when the strains cause micro-cracks that can be seen histologically. These can grow due to the structural characteristics of the bone tissue. This leads to the possibility of the bone weakening and the risk of mechanical failure. However, it is uncommon for cortical bone to fail in this way, as the cement lines of the secondary

osteons limit the spread of micro-cracks (Currey, 2002). The micro-damage is sensed by osteocytes, which signal to other osteocytes in a process called mechanotransduction. The osteocyte cell has up to 80 canaliculi, that reach can 15μm from the cell body, that sense damage and then stimulate a BMU to begin either modelling or remodelling.

Modelling can make bone stronger in two ways. First, by depositing bone to increase the cross-sectional area, the compressive forces are redistributed over a larger area. This reduces stress on the bone. Secondly, modelling can increase the bones resistance to bending and twisting by adding bone sub-periosteally. This is a particularly important response to loading in juveniles and manifests as periosteal apposition (Ruff et al., 1994; Bass et al., 1998; Lieberman et al, 2001; Lieberman et al., 2003). This modelling causes the bone to become more robust. More robust bones are more capable of resisting strains than more gracile bones are. Robusticity is the strength of a bone in relation to its shape and size (Stock and Shaw, 2007). There are several ways of calculating robusticity. The most commonly used method is a robusticity index, which compares diaphyseal thickness to the bone length. Another method uses beam theory based on the cross sectional geometry of the bone. However, this requires either a destructive cross section to be removed or expensive imaging to be taken. Stock and Shaw (2007) found that the external measures are strongly correlated with the internal cross sectional geometry. This means that the robusticity index is as good a method of assessing robusticity as the cross sectional geometry is, and has the added advantage of being non-destructive and simpler to implement.

Low levels of loading can also cause bone resorption by osteoclasts. Normally, a reduction in loading happens systemically caused by prolonged bed rest. This is because

that action of muscles results in the largest forces that affect bones (Frost, 1997). Additionally, localised resorption can happen if there are musculoskeletal changes that alter mechanical stresses in a region, such as amputation or immobilisation. According to Wolff's law (1892) the bone is resorbed to return the bone to its genetically determined shape. However, bone morphology is not just affected by genetics but also by its environment, including its interactions with muscles, and mechanical forces, over a long period of time. Another idea is that small-scale resorption occurs to remove excess mass from the skeleton (Pearson and Lieberman, 2004). The most likely hypothesis is that periods of resorption may be the pathological consequence of a lack of epigenetic stimulation (Dodd et al., 1999). Natural selection will not have mediated this trait because periods of low epigenetic stimulus are rare in non-hibernating animals. The magnitude of the strains that juvenile bones are exposed to has a great impact on the morphology of the growing bone. Juveniles who exercise regularly obtain a higher peak bone mass and a higher bone mineral density as young adults than non-exercising juveniles (Bradney et al., 1998). It has been shown that exercise has the largest impact on bone mass during puberty when hormone levels increase (Bass et al., 1998, 2002). Both oestrogen and testosterone influence bone growth. In response to strenuous mechanical loading juveniles deposit more sub-periosteal bone and reduce the rate of endosteal resorption. Newly active adults who had a sedentary childhood do not deposit significant amounts of sub-periosteal bone, but do reduce the rate of endosteal resorption (Ruff et al., 1994). Weight training leads to the formation of particularly strong and dense bones (Fujimura, 1997), which supports the theory that exercise induced strains lead to bone modelling. Thus, juveniles who were more physically active had greater cross-sectional robusticity than juveniles who were less physically active.

Most individuals attain their peak bone mass a few years after the long bone epiphyses fuse, normally in early adulthood (Heaney et al., 2000). Bone mass that is gained during childhood is often maintained throughout adult life. An individual with more robust bones as a juvenile will usually have more robust bones all through adulthood and into old age. Whereas, an individual with more gracile bones as a juvenile will usually have more gracile bones throughout life, and may be more at risk for osteoporosis in old age (Ferrari et al., 1998; Dertina et al., 1998). Individuals who have drastically reduced muscle use during the adolescent peak for bone deposition are unlikely to ever make up the deficit.

2.9 Histology

Bone is not simply one substance arranged in a particular manner. It is several materials that are combined to form basic bone tissue, calcium phosphate and hydroxyapatite. Further, this basic bone material is arranged in different mechanically relevant forms that make up trabecular bone and cortical bone, as well as primary and secondary bone (White et al., 2011). All of these types of bone structure have a different purpose and they can all be differentiated histologically.

Primary bone is usually deposited and calcified quickly in regions that had no bone tissue previously and at the site of fractures in order to form the first bony callous of the healing process. Layers of unorganised woven bone are deposited rapidly alongside unorganised collagen fibrils. When it is viewed under polarised light it appears to have a structure like woven fabric; hence its name (Scheuer and Black, 2000). There are large

spaces for a vascular network between the bone tissue. The primary bone is short lived and will soon be replaced by secondary bone.

Cortical bone is more organised then woven bone. It is composed of layers of lamellar bone sheets that are approximately 2-3μm across (Ascenzi et al., 1982). The lamellae are formed by the calcification of osteoid, which was layered upon existing bone surfaces, often woven bone (Martin et al., 1998). The calcification occurs along seams that are on average 15μm wide (Johnson, 1964). The process takes 10 days and results in the formation of three lamellae. During calcification, some osteoblasts are entombed within the lamellae and they differentiate into osteocytes. The chambers containing the cells are called lacunae. These have many small crack-like processes emerging from them, known as canaliculi. In well preserved archaeological bone the lacunae and their associated canaliculi can be seen histologically as small oblong fissures (**Fig 2.6**).

Occasionally, blood vessels can become trapped between the lamellae. This happens when periosteal vessels have new lamellae calcified over them. They are usually longitudinal and are known as primary vascular canals or primary osteons (Currey, 2002). These are unrelated to secondary osteons, although the terms osteon and Haversian system are synonymous. Primary osteons are not formed by remodelling activity, but by the formation of lamellae around a central canal without preceding resorption (Currey, 2002). Usually, the primary osteons are wedged between lamellae that bend around them. They have few lamellae of their own, and are much smaller than secondary osteons (Bright and Elmore, 1968; Chamay, 1970; Currey, 2002). In archaeological bone often only the central vascular canal can be visualised histologically.

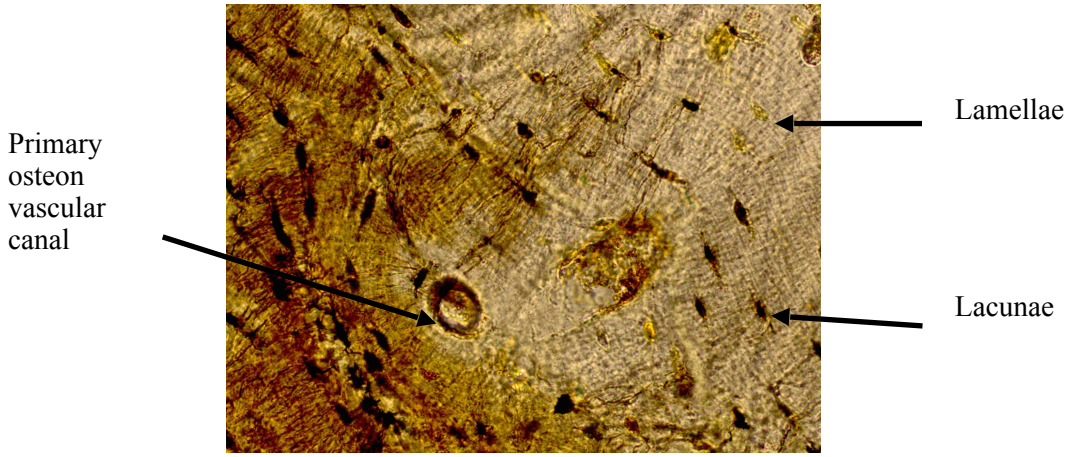

Fig. 2.6 Micrograph of a primary osteon.

Secondary bone is formed much more slowly and is a replacement for primary bone. The action of BMUs in the remodelling process causes the formation of tubular units called Haversian systems, or secondary osteons. Concentric rings of lamellar bone surround a central vascular canal, which is also known as a Haversian canal (Currey, 2002). Similar to primary lamellar bone, the lamellar rings have osteocytes in lacunae with canaliculi between their layers. The space between the lamellae is filled with extracellular matrix, which the canaliculi run through to connect the lamellae to one another and to the central canal. The osteocytes can communicate with one another via gap junctions on the ends of the cytoplasmic projections of the canaliculi (Currey, 2002). The osteocytes nearest to the blood vessels in the osteon canal exchange nutrients and metabolic waste with the blood. These cells then transfer the nutrients to neighbouring cells and collect their waste via the canaliculi (White et al., 2011). Histologically, secondary osteons are easily seen as a central canal surrounded by concentric rings of bone that are bounded by a solid cement line (Currey, 2002). In well preserved archaeological bone the lacunae and their canaliculi may be visible (**Fig 2.7**).

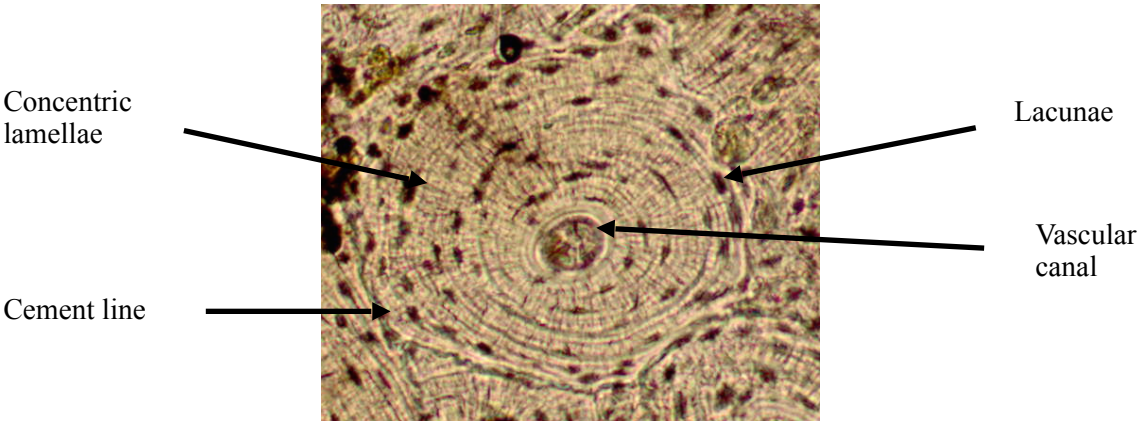

Fig. 2.7 Micrograph of a secondary osteon.

There are several types of secondary osteon that can be observed in human bone. Type 1 osteons are the common type of osteon that accumulate in the bone with age. Type 2, or embedded, osteons are small osteons that are contained within the lamellae of a larger osteon. Double-zonal osteons have a hyper-calcified ring surrounding them, which is caused by stress (Stout and Crowder, 2012). The final type of secondary osteon is a drifting osteon, which has continuous resorption on one side and continuous formation on the other. In addition to the different types of osteon, there are different morphologies of lamellae. The most common are the circular rings of lamellar bone, but there are also spiral lamellae, which overlap themselves, and crescent lamellae, which do not form a ring (Pazzaglia et al., 2012).

Compared to cortical bone, trabecular bone has a highly unorganised appearance. It is composed of many linked plates, called trabeculae, which are separated by unequal spaces. This arrangement makes trabecular bone much lighter than cortical bone (White et al., 2011). However, it is still optimised for strength as the trabeculae are arranged along lines of stress (Martin et al., 1998). Like cortical bone, there are osteocytes within the trabecular bone. They are irregularly placed within the trabeculae, and the canaliculi

pass them nutrients from the red bone marrow. The red bone marrow is located within the gaps between the bone.

2.10 Histological Age-at-Death Estimation

The potential to use bone histology to estimate age at death was first recognised when Balthazard and Lebrun (1911) discovered a correlation between age and mean osteon diameter in the midshaft tibia. However, the possibility of using bone histology to estimate age at death was not explored any further until the latter part of the 20th century (e.g., Kerley, 1965; Kerley and Ubelaker, 1978; Stout and Paine, 1992). The vast majority of the methods will only predict age at death for adults. Juvenile remains have been ignored until the present, with the exception of Streeter (2005).

The biological basis of the different methods are the same, whereby they are based on the changes that occur within the bone microstructure over an individuals lifetime. In particular the methods have focused on indicators of remodelling. These include osteon population density, secondary osteon morphometrics, Haversian canal morphometrics, and the number of primary vascular canals (Streeter, 2012). The quantification of these structures has been used to create several equations for estimating age at death (Robling and Stout, 2008). Researchers have sought to identify the sampling site that has the best correlation between histological changes and age and resulted in a proliferation of histological age estimation methods based on various different bones (e.g., Ahlqvist and Damsten, 1969; Singh and Grunberg, 1970; Rother et al., 1978; Thompson, 1979; Hauser et al., 1980; Fangwu, 1983; Thompson and Galvin, 1983; Cera and Drusini,

1985; Uytterschaut, 1985; Samson and Branigan, 1987; Drusini and Businaro, 1990; Narasaki, 1990; Ericksen, 1991; Stout and Paine, 1992; Kimura, 1992; Yoshino et al., 1994; Cool et al, 1995; Watanabe et al., 1998; Cho et al., 2002; Han et al., 2009; Martrille et al., 2009).

The majority of methods use a histological sample from one of the major long bones (see **Table 2.1** overleaf). The earliest method created regression equations from cross-sections of the midshaft of the femur, tibia, and fibula, for a sample of individuals that were aged between birth and 100 years (Kerley, 1965). It quantified intact and fragmented osteons, primary vascular canals, and unremodeled lamellar bone, in four ROIs at 100x magnification. A revision to the method accounts for the differences in field sizes between microscopes (Kerley and Ubelaker, 1978). Many of the later methods were based on this original work, but required smaller samples, in order to reduce the amount of destruction caused to the major long bones (Singh and Grunberg, 1970; Thompson, 1979; Thompson and Galvin, 1983; Narasaki, 1990; Ericksen, 1991; Han et al., 2009).

Some of the methods use histological samples from other bones. The histology of the clavicle and rib bones were used by Stout and Paine (1992) to estimate age at death. Their method produced regression equations for both the clavicle and the ribs, based on osteon population density. By sampling these bones it avoids using destructive sampling on any of the major long bones (Streeter, 2012). Additionally, rib histology is likely to be less affected by individual variations caused by activity and muscle use. However, the small area of cortex and high turnover rate of the bone may cause difficulties in analysing the sections.

Despite the large number of studies focusing on the histology of adult bone, there has been substantially less interest in juvenile bone. Some studies have described the histological features of juvenile bone (e.g., Streeter, 2005), but comparatively less is known about the histological changes that accompany age, compared to adult bone.

- Adult bone is characterised by indicators of *remodelling*.
- Juvenile bone is characterised by indicators of *modelling*.

This distinction between adult and juvenile bone is important for the current research project, because only one method has been developed previously to estimate age-at-death from juvenile rib histology (Streeter, 2005). There are four described phases, phase I is for juveniles that are less than five years, phase II is for juveniles of five to nine years, phase III is for juveniles of ten to seventeen years, and phase IV is for adults between eighteen and twenty-one. Each phase is associated with a description of the histological structures than predominate during the period. This type of methodology was used because osteon counts were found to have a poor correlation with age in juveniles (Streeter, 2005; Streeter and Stout, 2006).

It may be possible to produce a quantitative method of estimating juvenile age at death by using a long bone with a slower bone turnover rate. The method developed by Streeter (2005) produces a wide age range estimate. It relies on identifying which age category the histology most closely resembles, which could have a large inter-observer error rate. Developing a quantitative method may make it possible to give a more precise age estimation and could potentially reduce inter-observer error. Despite the

work of Streeter, the age related histological changes during the juvenile period have still not been examined to the same extent as the histology of adult bone.

Variable	Previous Findings (in adult bone)	Reference
Osteon population density	Denser in adults than juveniles.	Martiniakova et al., 2005
Secondary Osteon Area	Determined by the amount of bone that is removed by osteoclasts. Positively correlated with canal area.	Qui et al., 2003 Miszkiewicz, 2015
Secondary Osteon Minimum Diameter	Used to calculate osteon circularity. Osteons get more circular with age.	Britz et al., 2009 Hennig et al., 2015
Secondary Osteon Maximum Diameter	Used to calculate osteon circularity. Osteons get more circular with age.	Britz et al., 2009 Hennig et al., 2015
Secondary Canal Area	Positively correlated with osteon area.	Miszkiewicz, 2015
Number of Lacunae	Positively correlated with osteon population density.	Miszkiewicz, 2015

Table 2.1 Histological variables used in previous studies.

2.11 Summary

The first aim of this study is to map how bone microstructure varies with age. There have been few studies that have analysed the pattern of histological changes in juvenile bone. Most current histological data comes from the study of adult skeletons, both ancient (Erickson, 1976; Stout and Lueck, 1995) and modern (Skedros et al., 2005; Britz et al., 2009). Consequently, this study seeks to fill a gap in knowledge. This can be

achieved by studying both the primary and secondary osteons that are contained within the bone. By counting the number of osteons, and measuring their dimensions, it will be possible to produce a description of the way in which the bone structure changes with increasing age. As the current study will investigate children, this sequence will cover the shift in bone structure from primary bone to predominately secondary bone. This will further the understanding of microstructural bone growth.

The secondary aim is to produce a regression equation to predict juvenile age-at-death. This will be possible if any strong correlations between the histomorphological features of the humerus and age are discovered. In order to achieve this all of the histological variables will be tested for a correlation with age at death. The variables that have the strongest correlations will be entered into models that will predict age at death from the entered histological variables. The model that explains most of the variation will be used as a regression equation to predict juvenile age at death. Potentially, the regression equation could be applied to a bone fragment for use in cases that do not have a complete skeleton and so cannot rely on traditional age estimation methods.

The final aim is to investigate if inferred activity during life can influence the bone microstructure. The microstructure of the tibia and femur are likely affected by locomotion. The humerus was selected for this study as it is not as affected by locomotion. Hence, the humerus is more likely to exhibit difference between individuals that relates to different activities. The level of activity will be inferred from the degree of robusticity of the humerus. All of the histological variables will be compared between more robust children and more gracile children. This part of the study will be based on a subgroup of age-matched children.

CHAPTER 3.

MATERIALS

3.1 Introduction

This chapter will introduce the skeletal sample that was used in this study. It will cover the selection criteria used to select the sample. It was important to formulate selection criteria at the beginning of the study so that the sample could best fulfil the aims of the study. Following this, there will be an overview of the age-at-death distribution in the sample. The demographic of the sample differs from the demographic of the population that it was drawn from, because only juveniles were included. This means that the sample is only representative of the juvenile population and is not representative of the entire population. Lastly, there will be an archaeological background. This will include a brief history of the site of excavation of the skeletal remains, a summary of the remains that were found at the site, and the burial conditions.

3.2 Selection Criteria

There were several criteria that a skeleton had to meet in order to be included in this study. This study sought to investigate the histological changes in the humerus that occur with increasing age. As such the most important criterion was that an estimation of age at death was be possible. Furthermore, it was important that the age estimation was as accurate as possible, so to this end, multiple methods of estimation were used.

This was important so that any histological patterns that emerged were accurately linked with age. Any skeletons that could not be aged were excluded from this study.

Linked to the first criterion is that the skeletal remains must all be those of individuals who died within the juvenile period. This is the time from birth until 18 years of age. This study specifically looked at the histological patterns during the juvenile period, because juvenile histology has been much less studied than adult histology. Any skeletons that were estimated to have died after 18.9 years of age were excluded from this study.

The third criterion was that a humerus was present for each set of skeletal remains, but it did not necessarily have to be intact or complete. In juveniles the epiphyses are not yet fused onto the diaphyses, and in younger individuals they may not have even appeared yet. Combined with their small size, this means that the epiphyses are frequently not excavated along with the rest of the skeleton. Additionally, taphonomic processes may have damaged or broken the bone. This study only covered the histology of the humerus, specifically the anterior midshaft region. Consequently, provided that this particular region of the humerus was present in the remains then that skeleton was included in this study. Preferably the humerus would be intact so that robusticity indices could be calculated from the bone. However, investigating histological variation with robusticity was secondary to investigating the variation with age, so a robusticity index was not essential.

The final criterion was that the humerus must not have any evidence of pathology. It has been noted that chronic illness can reduce the rate of bone growth in children, and there

are numerous studies that link poor health to reduced stature (Boersma and Wit, 1997). For an infection or disease to cause a bony reaction it must be a long running process. Due to the chronic nature it is possible that not only the macroscopic growth has been affected but also the microscopic growth of the histological features. Further to this, it is likely that any reactionary bone growth could obscure the visualisation of the histological features. For these reasons, any pathological specimens were excluded from this study.

3.3 Sample

The study sample was composed of the skeletal remains of juveniles. These are individuals who died before reaching adulthood. The age range is from neonatal to 18.9 years. The skeletons were placed into one of four age classes. These were infant, 0-2 years, early child, 3-7 years, late child, 8-12 years, and adolescent, 13-18 years. They can be seen in **table 3.1**, which also includes a break down of the estimated age at death ranges. Each age class includes juveniles up to the maximum age within their class. Therefore, the 0-2 class includes skeletons aged 2.9 years, the class aged 3-7 includes skeletons aged 7.9 years, the 8-13 class includes skeletons aged 13.9, and the 14-18 class includes skeletons aged 18.9. Age classes were used due to the inability to gauge chronological age from the archaeological remains. The classes are based on the developmental age of the skeleton rather than the true chronological age. Due to the sample being solely juveniles, no attempt was made to sex the individuals.

	0-2	3-4	5-7	8-10	11-12	13-15	16-18	Total
Infant	5	0	0	0	0	0	0	5
Early Child	0	22	17	0	0	0	0	39
Late Child	0	0	0	17	10	0	0	27
Adolescent	0	0	0	0	0	8	4	12

Table 3.1 Age classes in the sample, and the smaller age groups from the age estimations.

All of the specimens had been excavated from the St. Gregory's Priory site in Canterbury, Kent. This is a monastic site that dates to the late medieval period. The priory and its associated graveyard were in use for around 400 years (Hicks & Hicks, 2001; Miszkiewicz, 2012). Consequently, the excavated skeletons do not necessarily date to the same time. Additionally, all of the remains are those of unknown individuals, as there are no known burial records. However, the identity of some individuals has been inferred from their burial location within the priory and their associated grave goods. It is believed that some of the remains are those of former priors.

It is possible to infer the socioeconomic status of the individuals based on the location of their burial (Hicks & Hicks, 2001; Tatton-Brown, 1995). Some of the remains were excavated from within the priory foundations. These burials most probably represent higher status individuals, who had more money and better diets, and undertook less strenuous activity than the majority of the society. Most of the burials were excavated from the cemetery, where the ordinary and lower status people were interred. This study includes juveniles who were excavated from both the priory and the cemetery, and the breakdown of this is shown in **table 3.2**.

	Priory	Cemetery	Total
Infant	1	4	5
Early Child	8	31	39
Late Child	4	23	27
Adolescent	1	11	12
Total	14	69	83

Table 3.2 Burial location, split by age class.

3.4 Archaeological Background

All of the skeletal material was excavated from St. Gregory's Priory, Canterbury, Kent by the Canterbury Archaeological Trust. The excavation took place from 1988 to 1991. There were 1342 articulated skeletons excavated during this time, and curated at the University of Kent. The site has been dated to the late medieval period, specifically, the 12th century to the mid 16th century. The remains represented a wide age range, including foetal, infant, juvenile, and mature adult individuals of both sexes. A small number of the burials were contained within the priory itself, while the majority of burials were within the associated cemetery. It is likely that the priory burials represent individuals who had a high social status during their lifetime, for instance, priors or wealthy individuals (Hicks and Hicks, 2001).

St. Gregory's Priory has had a varied history. Archbishop Lanfranc commissioned a church to be built in 1084 AD, which would later become St. Gregory's Priory. The original church was a modest size and based on a Norman design. It comprised of just a simple nave and chancel. Lanfranc himself was from Normandy, and he was appointed

by William the Conqueror to reform the church (Clover and Gibson, 1979). Lanfranc was also charged with restoring Canterbury Cathedral and nearby St. Augustine's Abbey. Additionally, he built a leper hospital at Harbledown, which is a short distance from Canterbury, and the nunnery of St Sepulchre in the outskirts of the city. The church of St. Gregory was built as an adjunct to St. John's Hospital, which was located on the opposite side of the road, and cared for the poor, infirm, lame, and blind. The church was established to care for the sick of the hospital and provide free burials for the poor. Both the church and the hospital were located just outside the city walls.

The church was upgraded to a priory in 1133 when Archbishop William of Corbeil appointed Augustinian canons in place of the clergy. At this time the priory was expanded. A choir was added, as well as a new larger chancel, and transepts on the north and south sides which each led to a twin celled chapel. Shortly after the expansion work was completed, a fire severely damaged the building. As a result of this Archbishop Theobald commissioned a much larger and grander priory to be built on the site. The priory church was rebuilt as a larger building, and an extensive claustral complex was constructed to the north of the church. The complex included a chapter house, undercroft, dormitory, and infirmary. The church was completed first, in 1181, and the complex was completed later, in 1225. The Prior's Lodge and a kitchen were additional buildings that were added to the site in around 1250. This marked the end of the large scale building work at the Priory (Hicks and Hicks, 2001).

However, small additions and modifications were made over the following 300 years. This included buttressing the church walls and the addition of two towers, as well as minor reorganisation of the internal walls. The conjectural reconstructions in **Fig 3.1**

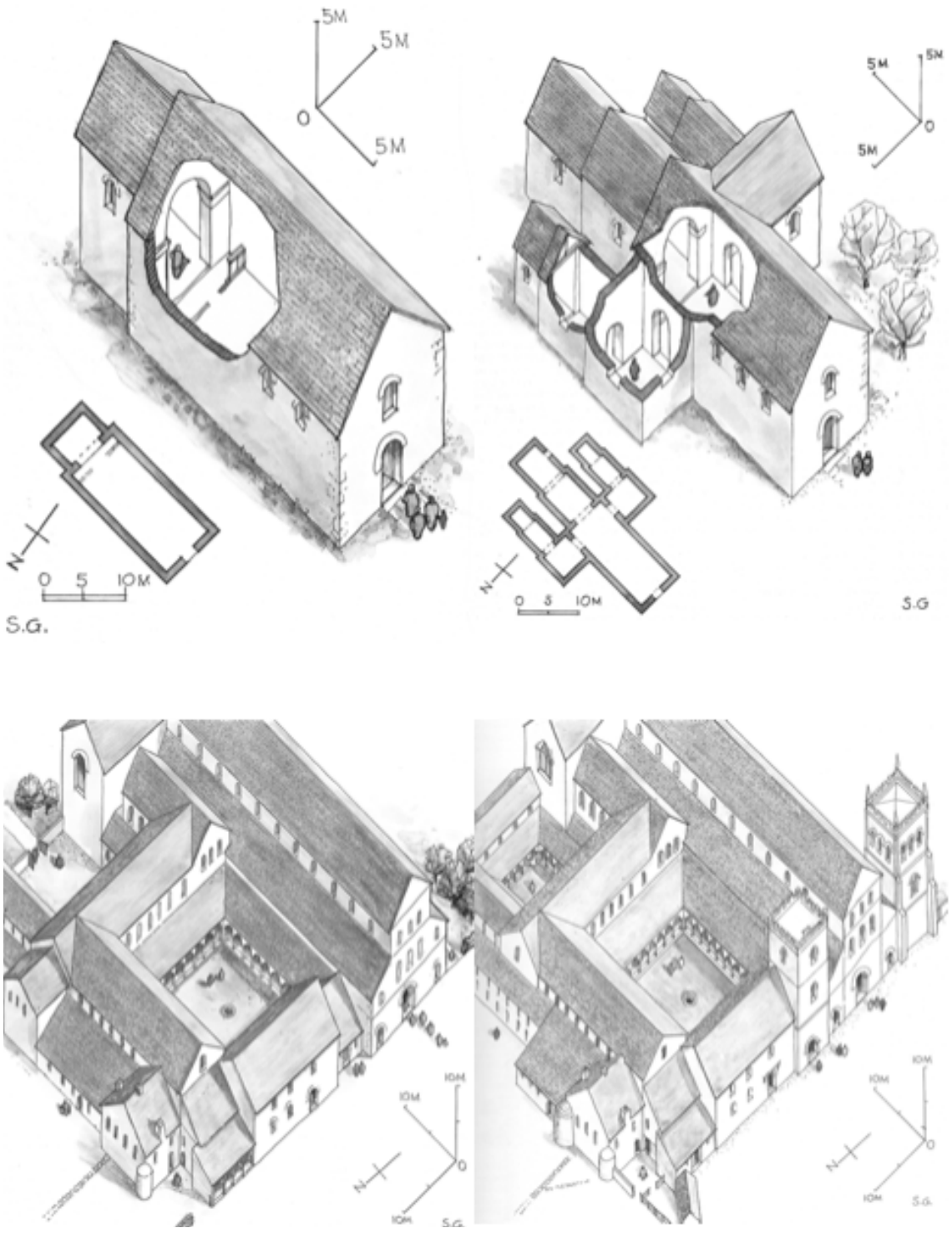

Figure 3.1 The expansion of St. Gregory's priory. Top row left to right: 1084; 1133. Bottom row left to right: 1225; 1250. Images reproduced from Hicks and Hicks (2001).

show how the Priory was altered over the course of its existence. In 1537 St. Gregory's Priory was dissolved according to the orders of King Henry VIII. Consequently, all of the priory buildings were destroyed, with the exception of the prior's lodge, which was converted into a private residence. The lodge was removed to make way for an army barracks in 1848. Eventually, the barracks was also replaced by houses and later a post office. (Hicks and Hicks, 2001).

The overall preservation and condition of the skeletal material is good (Anderson and Andrews, 2001). Many of the skeletons were almost complete, and had well preserved bones that showed limited taphonomic damage. 40% of the skeletons had at least three quarters of their bones present, and only 20% of the skeletons were fragmentary. The juvenile skeletons in the assemblage were as well preserved as the adult ones. While the overall standard of preservation was mostly good, there were some graves that had been interfered with and the skeletons damaged. Several of the burials had been cut into by later burials that overlapped them, and a couple showed evidence of grave robbery. Given the good condition and completeness of many of the skeletons, it is surprising that around 90% of the individuals were buried without coffins. Of those that were buried in coffins these were made of stone, or less commonly wood. Lanfranc's Monastic Constitutions provides evidence that people were clad in a shroud before being laid directly into their graves (Knowles, 1951).

There are many factors that influence how well bone is preserved including both intrinsic and extrinsic factors. The intrinsic factors include the morphology and chemistry of the bone, as well as any pathological changes to the bones structure. The extrinsic factors include botanical infiltration, freeze-thaw, chemical erosion, pressure,

scavengers, and human activity (Henderson, 1987). At St. Gregory's Priory the soil that the skeletons were buried in was mainly composed of clay, with some chalk and flint. The degree to which bone is preserved depends on the pH of the clay it is buried in. The clay at this site was only slightly acidic, so it only caused limited chemical erosion. Chalk soils can cause bones to become both fragile and eroded (Brothwell 1972), and may make them harder to clean. Fortunately, there was only a small amount of chalk in the soil so it had a minor effect.

Overall, around one quarter of the individuals had died before reaching adulthood. Of those that died as juveniles the greatest mortality was between the ages of one and six. 45% of the juveniles died when they were in this age range. However, in the cemetery, sub-adult mortality rose to around 40%. This is significantly higher than for those buried within the priory; sub-adult mortality in the priory is around 8%. The level of sub-adult mortality at St. Gregory's Priory is similar to that found in other medieval sites, such as Hartlepool (Birkett, 1986) and St. Andrew, Fishergate (Stroud and Kemp, 1993).

CHAPTER 4.

METHODOLOGY

4.1 Introduction

This chapter will cover the methodology that was used in this study. It will begin with the criteria that were used to choose the sample. It will then cover the macroscopic methods that were used, including methods of age at death estimation and method of calculating robusticity. Following this, the microscopic methods will be explained, including the methodology of histological slide preparation, imaging, and measurement of histological features. The chapter will conclude with information about the type of analyses that were undertaken.

4.2 Sampling

In total 83 skeletons were included in this investigation. These all had to fulfil particular criteria before they were accepted into the study. The first criterion was that the remains must be those of a juvenile. This is an individual with an age-at-death of less than 18 years. This age range was selected because it is only the growth of the humerus that is being investigated, and growth is usually complete by the end of the juvenile period. The second criterion was that the remains had a humerus present. This would permit all of the macroscopic measurements to be taken, as well as the sections for the histological sampling. Secondary ossification centres were not always present because they are

frequently destroyed by taphonomy or not recovered. The third criterion was that an age at death could be estimated for each of the skeletons. This would allow for the formation of age categories so that a histological series could be produced for the entire juvenile age range, and that patterns of variation could be seen throughout the ages. It would also allow for the individuals of different robusticities to be compared for each of the ages. The last criterion was that the skeletons had to have no visible pathology present, with no evidence of bony infection or reactive bone growth. It may be possible that a child with evidence of disease may have an altered growth pattern (Sherwood et al., 2000). Diseased bone could also impair the visualisation of histological features.

4.3 Macroscopic Methods

4.3.1 Age Estimation

Producing an age at death estimation for skeletal remains is a complex process. There can be large individual differences in the developmental age between skeletons with the same chronological age. These differences can be caused by a range of intrinsic and extrinsic factors, including genetics, diet, and activity. This confounds the ability to produce an absolute age at death estimate. Instead, individuals are given an age range, for instance 2-4 years, or an age class, for instance, early child. All of the skeletons in this study were given an estimated age at death and an age class. This study uses the age classes infant, early child, late child, and adolescent. Infants are considered to be newborns until reaching 2.9 years of age. The early child class covers children between the ages of three years and 7.9 and the late child class covers children aged from eight

until 13.9 years. Children from 14 years of age until 18.9 years of age are included in the adolescent class.

Up to five different methods were used to assign an age at death estimate to each set of skeletal remains. Some of the skeletons were lacking the necessary elements to perform all five methods, but most were complete enough for all of the methods. By using multiple methods a more reliable estimate is produced (Lovejoy et al., 1985). The methods used are based on several developmental changes in the body. These are; the development of deciduous and permanent dentition, the fusion of ossification centres, and the growth of the long bones. The appearance of the secondary ossification centres was not used in this study as they were rarely recovered.

The development of the teeth and the timing of tooth eruption are more closely associated with chronological age than the fusion of the epiphyses and bone growth (Ubelaker, 1987, 1989; Cardoso, 2007). As such, tooth development is likely to be subject to a greater degree of genetic influence than the other elements. Due to this, the methods of age estimation that are based on the teeth produce more accurate estimations of age at death than the methods based on bone growth (Lewis and Garn, 1960; Demirjian, 1986; Smith, 1991; Bowman et al., 1992). Accordingly, in this study most weight was given to the methods that are based on the teeth. The methods that rely on long bone growth are the least exact (Saunders and Hoppa, 1993), and so they are the least relied upon in this study.

The first method that was used is Ubelaker's (1989) dental development chart. This estimates the age at death based on the stages of development and eruption of all of the

teeth along the dental arcade. This method is the least precise out of all of the methods as it provides an estimate based on an overview of the development of all the teeth. There is some variation between the stages of attainment between individuals and the eruption sequence itself may vary (Smith and Garn, 1987). However, this method can be a useful initial estimate of the age at death.

The second method is also based on the dentition. Smith (1991) compiled a table detailing the average age of attainment of different growth stages of all of the teeth separately. It is based on the work by Moorrees et al. (1963). The growth stages that are included cover the formation of the root and crown, and eruption of the tooth. The only stages that are included for the deciduous dentition are the root completion and the crown completion. However, for the adult dentition all stages of development were included:

- Cusp initiation
- Cusp coalescence
- Crown outline complete
- Crown one half
- Crown three-fourths
- Crown complete
- Root initiated
- Root cleft present
- Root one-fourth
- Root one-half
- Root two-thirds
- Root three-fourths

- Root complete
- Root apex half closed

To use this table the individual tooth must be identified first. Then the developmental stage can be assessed and a mean age of attainment taken from the table. This process was repeated for all of the available teeth for all of the individuals. There is a table for each males and females, but since the skeletons in this study are not having their sex estimated, separate estimates from each table were made and then averaged. This will be an approximation of the age at death of the individual.

The state of fusion of the epiphyses was the next method to be used. McKern and Stewart (1957) created a chart of the skeleton accompanied by a list of the major secondary ossification centres and the average age at which they fused to the diaphyses. They also included tables that showed the likelihood that a particular element was fused at a particular age. This is important because there is some variability in the chronological age at which the elements fuse (Cardoso, 2005). Some of the intervals between the stages are quite large, so this method usually results in an age range spanning a few years as its age at death estimation.

The final two methods are both based on the growth of the long bones. For both of these methods it is necessary to measure the diaphyseal length for all of the long bones that are present. This is the length of the diaphyseal shaft between the growth plates at either end. It is measured using an osteometric board. Each measurement can then be checked against the growth chart for the particular bone that it came from. This will produce a series of age estimations, one from each bone. These give the likely age range of the remains. Both methods have skeletal growth profile charts that differ slightly as they are

based on different sample populations. Hoppa (1992) produced tables that are based on modern Caucasian growth values, but it also includes growth curves based on archaeological data. However, the archaeological data was produced from skeletons that were aged by dental development. Unfortunately their chronological age is not known. Maresh and Beal (1970) produced tables that are based solely on modern children from Denver, Colorado. This means that they may not provide accurate estimations of the age of archaeological remains if the growth rates do differ between populations (Schillaci et al., 2011). Due to this, the charts by Hoppa (1992) are more likely to provide an accurate age estimation.

4.3.2 Measurements

The standard measurements that are described by Buikstra and Ubelaker (1994) were taken using an osteometric board and digital callipers. These measurements were the length of the humerus, the maximum breadth of the mid shaft humerus and the minimum breadth of the mid shaft humerus. The maximum length is measured from the most superior point on the humeral head to the most inferior point on the trochlea (Buikstra and Ubelaker, 1994). Many of the humeri did not have the epiphyses present, so in these cases just the diaphyseal length was measured.

Whether a skeleton is gracile or robust can be calculated by using a robusticity index (Stock and Shaw, 2007). This compares the length of a bone to its width and uses the measurements of the humerus that are detailed above. The robusticity indices have been used as a proxy for the level of activity that an individual underwent during their lifetime (Trinkaus, 1983; Currey, 1984; Martin and Burr, 1989; Pearson, 2000), though

multiple factors likely influence robusticity unrelated to behaviour, such as genetic predisposition. It is calculated by the formula:

$$\frac{(\text{maximum diaphyseal breadth} + \text{minimum diaphyseal breadth})}{\text{Bone length}} \times 100$$

In this study, the individuals were split into three equally sized robusticity groups based on their robusticity indices relative to one another. These were a low, a mid, and a high robusticity group. By splitting the sample in this way it was possible to compare the groups within each age class, using one way ANOVAs. The raw indices were retained for use in Pearson's correlations.

The length of the radius, ulna, femur, and tibia were also measured using an osteometric board. These measurements were used in the age at death estimation methods (Maresh, 1970; Hoppa, 1992), and also to estimate the height of the individuals. This was achieved by entering the long bone lengths into the regression equations devised by Ruff (2007).

4.4 Microscopic Methods

4.4.1 Sectioning

The method of obtaining a histological section used in this study is based on the methodology of De Boer et al. (2010). There are several differences between the two methods. The method used in this study is more mechanised. By using cutting and grinding machines the process is more efficient and has a reduced possibility of

producing an uneven section. Additionally, in the method used in this study, the section is affixed to a glass slide much earlier in the process, which gives it greater stability. The sections in this study are not stained in any way. This further reduces the production time.

1. To cut a section from the bone it must be orientated and put in a vice to hold it steady while sawing. Mark the bone with pencil as a guide to where the section is going to be taken from. In this case it is the anterior midshaft region. Use a dentist's saw to remove the sections from the bone.
2. Coat the inside of a plastic specimen cup with release agent to ensure that the section can be removed easily after it has been embedded in resin.
3. Place the cut section into the specimen cup in the correct orientation. Use a specimen cup that is only slightly larger than the section to minimise the amount of resin that must be cut off later.
4. Use a balance to measure five parts epoxy resin to one part epoxy hardener into a small glass vial. Mix this together with a spatula for approximately three minutes, until the mixture has turned clear. If the incorrect ratio is used, or it is insufficiently mixed, it will be either too sticky or too hard to be cut. While using the resin, gloves should be worn to protect the skin.
5. Pour the mixture slowly into the section in the cup, taking care not to move the section. Pour enough in so that the section is just covered by the resin. This will minimise the amount of resin that must be cut off later. Leave the resin to harden for 24 hours.
6. Once the resin is fully hardened, the block containing the section can be removed from the section cup. If enough release agent was used then it should slide out easily.

7. The section is now ready to be cut into slices using the IsoMet precision saw. Hold the section in a chuck to keep it steady during the cutting. Line up the diamond-wafering blade with the desired thickness of the slice and start the blade spinning at 100 rpm and raise it to 300 rpm once the blade has bitten into the section. If the section is cut obliquely it may obscure the osteon morphology.
8. After the section has been cut it can be mounted on to a glass slide. To begin, grind the side of the section that will be mounted using abrasive paper with a grit of 600.
9. Polish the section using a finer grit of abrasive paper, 1200.
10. Rinse with water to remove any loose particles and allow it to air dry.
11. Clean slide using a cotton swab with 100% ethanol and allow it to air dry. This will remove any particles that are on the slide that could obscure the histological features.
12. Mix a small amount of epoxy resin and hardener using a plastic spatula. This will begin to harden approximately 30 seconds after it is fully mixed.
13. Apply the resin to the polished side of the section and use the index and middle fingers to press the section down on to the slide firmly until the resin has spread evenly. The resin will be completely dry in an hour. The embedded section should now be affixed to the glass microscope slide.
14. Following this, cut any excess thickness off with the IsoMet saw. The slide should be placed in a chuck to hold it steady. Start the blade spinning at 100 rpm and raise it to 300 rpm once the blade has bitten into the section. This will minimise the time that has to be spent grinding the section down.
15. Grind the section down using an EcoMet grinder - polisher mounted with silicon carbide paper of grit 320. The abrasive paper should be kept wet throughout to prevent a friction buildup that could damage the section. The section is held in place

with a histolic precision grinding fixture to prevent over grinding. Check the section regularly to prevent it from being ground too thin and use a microscope to check the progression of the section.

16. Once the section has been ground to the desired thinness, approximately 50-100µm, it should be polished with 0.3 micron micro polish on a polishing cloth that is mounted on an EcoMet grinder - polisher. This should also be kept wet. Polish the section for approximately two minutes to remove any surface scratches that may be left from the abrasive paper. Rinse any remaining polish off with water.
17. Place the mounted section into a glass beaker that is one quarter filled with water, and place the beaker into a half filled ultrasonic water bath. Set the water bath to vibrate for two minutes. No heating is required. Spray ionised water onto the section at 30 second intervals. This will remove any particles that are on the surface of the section. Let the section completely air dry.
18. Dip the section into a beaker of 95% ethanol for two minuets. Let the section completely air dry. The ethanol will dehydrate the section.
19. Dip the section into a beaker of 100% ethanol for two minutes. Let the section completely air dry.
20. Dip the section briefly into a beaker of histoclear twice. Let the section completely air dry.
21. Prepare a slide cover by wiping it with 100% ethanol and allowing it to air dry.
22. Apply DPX mounting medium to the exposed surface of the section and slide over an area approximately the same size as the cover slip.
23. Press the coverslip gently on to the DPX covered slide and wait for the DPX to spread and seal the edges of the cover slip. Once this is completely dry the slide is ready for imaging.

4.4.2 Microscopy

It is impossible to see the microstructure of bone without using a microscope. The microscope is designed to magnify and to resolve a small object so that its characteristics can be observed and measured (Stout and Crowder, 2012). Since this project is based on microscopy it is necessary to understand how the microscope functions.

The resolution refers to when the closely spaced features are differentiated from one another. The human eye can only resolve objects that have a distance of 0.1-0.2 mm between them, and this is the resolving power of the eye (Croft, 2006). The resolution of features that are more closely spaced than the resolving power of the eye must be resolved using a microscope (Slayter and Slayter, 1992). Additionally, there must be enough contrast between the feature and the surrounding material for the feature to be visible (Bradbury and Bracegirdle, 1998) without the need for a stain. Bone is a pale yellowish brown with darker features, so it is not necessary to use a stain for the majority of histological methods.

The modern microscope works in a similar way to the first microscopes. The first compound microscopes was made by Hans and Zacharias Janssen in the late 16th Century in the Netherlands. It was a simple tube with a lens at either end of it. It could be lengthened or shortened to alter the magnification. In a compound microscope there are two lenses that work in conjunction to produce a magnified image. This basic design is still present in modern microscopes. Previously, microscopes only had a single lens, which was incapable of magnifying to the same extent as a compound microscope (Smith, 1994). The earliest compound microscope was capable of magnifying an object

by up to ten times, while some current microscopes can magnify up to 2000 times. Over the centuries the basic principle of the compound microscope has remained the same, but the housing of the microscope has got increasingly more complicated.

In modern microscopy the light from the light source is condensed and focused on to the specimen. This results in the bright and even illumination of the specimen, which can improve the resolution of the virtual image. The objective lens is closest to the specimen and the distance between the two can be altered to focus the image (Cho, 2012). There are usually several different objective lenses that each have a different magnification power. On the microscope used in this study there are objective lenses of 2x, 4x, 10x, 20x, 40x, and 60x. The other lens is the eyepiece lens, which has a magnification of 10x. This lens can also be focused. Some microscopes, including the one used it this study, are equipped with digital cameras that are linked to computers. Software can be used to measure the length and area of the microscopic structures, as well as to count them. However, this does not replace the direct observation of the specimen, and the virtual image through the microscope should be referred back to regularly.

As more information was discovered about the physics of light, more powerful microscopes were manufactured. Improvements were made to the magnification, resolution, colour correction, and the illumination of the object. Light is a form of energy that moves in continuous waves, and is a part of the electromagnetic spectrum. Visible light is in the part of the electromagnetic spectrum that has wavelengths between 750 and 400 nm; this is the only part of the spectrum that is visible to the human eye (Cho, 2012). The wavelength is the distance between two waves when measured at the same point on each wave. The brightness of the light is the result of the amplitude, or

height, of the wave (Murphy, 2001). The different wavelengths within visible light all correspond with different colours that can be seen.

The lenses in microscopes are composed of transparent glass or plastic that bends light in a predictable way. The diameter of the lens is related to the magnification. A smaller lens diameter will bend light more, which creates a larger image, and therefore a higher magnification. By knowing the focal length of the lenses, and the size of the lens diameter, the size of the magnified virtual image can be calculated. A virtual image is one that can only be seen through a microscope. The greater the magnification that is used, the lower the resolution of the virtual image will be. The reduction in resolution is caused by light diffraction through the microscope (Cho, 2012).

4.4.3 Imaging

The imaging of the histological slides is achieved by using an Olympus BX51 microscope that is mounted with a DP25 olympus camera. The camera is connected to a computer that can receive live microscopic images. The software programme CellD was used to examine the images. Images were taken at five regions of interest, or ROIs, from the section. These are (as seen in **Fig 4.1**), the medial periosteal surface (1), the antero-medial periosteal surface (2), the anterior periosteal surface (3), the antero-lateral periosteal surface (4), and the lateral periosteal surface (5). This array of images provides comprehensive coverage of the whole section.

These particular regions of interest were chosen because it provides an unbiased method of choosing the ROIs. This will improve the reliability of the study. Villa and Lynnerup (2010) discovered that there was no significant difference between the ROIs, for either

intra- or inter-section variability. This means that the location of the ROIs will not affect the results of the investigation. They also showed that the intra-section variability was higher with age, although not significantly, but this should not affect the study of juvenile bone. Furthermore, having this many ROIs means that a large proportion of the cross section is analysed. In the some cases the entire half cross section was covered by the ROIs.

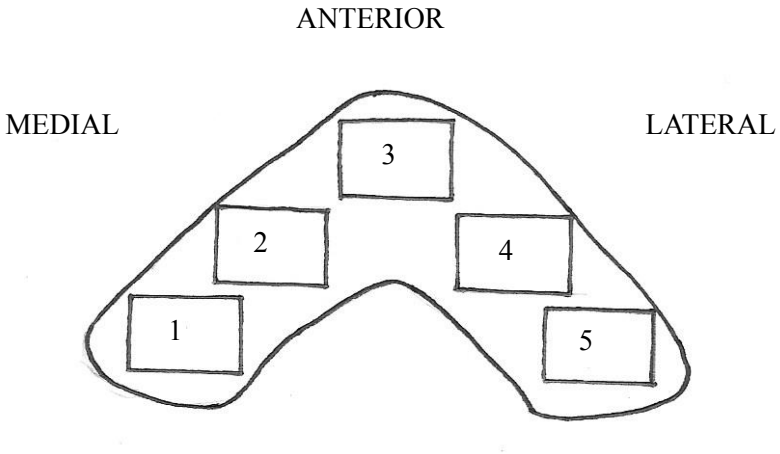

Fig 4.1 Regions of interest on the anterior humerus section.

Several histology variables were selected for this study. The variables that were measured are:

- Number of osteons
- Number of primary osteons
- Number of secondary osteons
- Primary osteon canal area
- Primary osteon canal minimum diameter
- Primary osteon canal maximum diameter
- Secondary osteon area
- Secondary osteon minimum diameter
- Secondary osteon maximum diameter

- Secondary osteon canal area
- Secondary osteon canal minimum diameter
- Secondary osteon canal maximum diameter
- Number of lacunae

Each of the five regions of interest was imaged at 10x magnification. The number of osteon canals is counted from this image and from the virtual microscope image. Primary osteons are identified by a circular canal that is surrounded by few, if any, circumferential lamellae. They do not have a cement line (Currey, 2002). Secondary osteons are identified by a circular canal that is surrounded by many circumferential lamellae and bordered by a defined cement line (Currey, 2002).

From the numbers of osteons, the osteon population density can be calculated, as well as the primary osteon population density, and secondary osteon population density. The osteon population density is calculated by dividing the total number of osteons that are counted by the area of the ROI. In this study, at 10x magnification the area is 2.24mm^2. This is repeated using the number of primary osteons to calculate the primary osteon population density, and the number of secondary osteons to calculate the secondary osteon population density. Using population density is preferable to the raw number because it is not dependent on the size of the ROI. This makes it simple to compare different data sets.

Each of the regions of interest (**Fig. 4.2 a**) are split into quarters so that they can be imaged at 20x magnification, as seen in **Fig 4.2 b**. This results in four sub-ROIs per ROI. At this level of magnification the dimensions of the primary and secondary

osteons can be measured. The measurements include the area of each primary osteon canal, secondary osteon and, secondary osteon canal can be measured. Both the primary and secondary canal maximum and minimum diameter can also be measured, as well as the maximum and minimum diameters of the secondary osteons. The measurements are all taken in μm using the software in CellD.

Following this, each one of the four 20x magnification images was then also split into four further areas that were imaged at 40x magnification. This results in sixteen areas per ROI, as seen in **Fig 4.2 c**. At this magnification it was possible to count the number of osteocyte lacunae that were present. However, it was not possible to visualise the lacunae in all of the ROIs. In many of the sections it was impossible to visualise any lacunae in any of its ROIs. This was due to the poor preservation of these structures in the sampled juvenile bone.

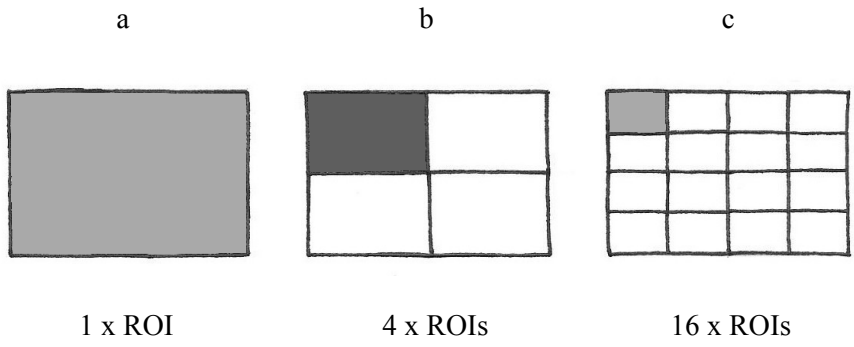

Fig. 4.2 Magnification of regions of interest.

Once the data has been collected from each ROI, the average value for each variable for every individual is calculated. This is to simplify the analyses and to reduce the variation between the ROIs of an individual. All of the measurements that were taken at the four 20x sub-ROIs were averaged to produce a single value per variable for each of

the five ROIs across a slide. Additionally, the number of lacunae was averaged across the sixteen 40x magnification areas to provide a value for each ROI. Finally, the average of all of the values for each variable was calculated from the average values of each of the five ROIs. This resulted in a single value per variable for each slide.

4.5 Analyses

The data was analysed using the software programme Statistical Package for the Social Sciences (SPSS version 22). All of the data was entered into the spreadsheet and coded into variables, so that it could be tested statistically. Each individual was associated with its skeleton number to keep track of the data.

Descriptive statistics were used first to summarise the data and test for normality (Brace et al., 2009). Measures of central tendency were tested for each of the variables. These included the mean and standard deviation, the median, and the mode. The results of these describe the distribution of the data for each variable. Following this, a test of normality was used to check whether the data conformed to a normal distribution curve. In this case a Levene's test was used. The result of this test indicates whether a parametric or non-parametric inferential test should be used on the data. If the data displayed a normal distribution then a parametric test should be used, but if the data was not normally distributed then a non-parametric test should be selected (Brace et al., 2009).

All of the variables were shown to have a normal distribution so a parametric test was appropriate. In order to compare how the variation of the dependent variables is caused by the independent variables a test to compare the means was used. This was a one way ANOVA. These were performed to compare how the number and size of osteons varied between the age classes. Following this the same variables were compared for each of the robusticity groups. If an ANOVA indicated that there was a significant difference between the groups, Tukey's post hoc tests were performed. This test would show which of the age classes or robusticity groups differed significantly from the others.

If an ANOVA and Tukey's post hoc test revealed a significant difference between any of the groups, Spearman's rank correlations were performed. The correlations were used to gauge the strength of the relationship between the variable. Spearman's rank correlations were used because the age of the individuals in this set of analyses is given in year ranges, rather than a single age for each skeleton.

The final analysis was regression analysis, both linear regression and multiple regression. This would produce a regression equation to predict age at death from the bone histology variables. In this set of analyses, the age-at-death for each skeleton was used, rather than an age class. First, the strength of the relationship between the variables was assessed using Pearson's correlations. Then the linear regression analysis was performed on the primary osteon population density and the secondary osteon population density separately. Finally, both primary and secondary osteon population density were included in a multiple regression.

CHAPTER 5.

RESULTS

5.1 Introduction

The aim in this chapter is to determine if the frequency and size of primary and secondary osteons vary with age. Osteon variation with robusticity is also examined. Finally, regression analysis will indicate whether a regression equation can be used to predict age at death from bone histology.

The analyses are undertaken in four steps. Firstly, the data were subdivided into four age classes, and then summarised using descriptive statistics. These included measures of central tendency (mean, median, and mode) and measures of dispersion (range, maximum and minimum, and standard deviation). All of the data was tested for normality using a one sample Kolmogorov–Smirnov test. The data showed a normal distribution for all variables. Only significant results will be reported in this chapter.

Second, the frequency and size of primary and secondary osteons were compared between the age classes using one way ANOVAs. The ANOVAs were conducted with Tukey's post hoc tests to determine which classes differed from one another. Following this, Spearman's rho were performed to assess the strength of the association between the frequency and size of osteons, and the age classes.

Third, the robusticity of the children in the age class of two to seven years was assessed using one way ANOVAs. These ANOVAs were also conducted with Tukey's post hoc tests to find out which groups differed from one another. Further Spearman's rho were performed to assess the strength of the association between the frequency and size of osteons, and the robusticity categories. For the second set of ANOVAs, which tested the variables against robusticity, only one age group was used. This was so that the affect of age on the results could be limited as much as possible.

Fourth, the variables that were most strongly associated with age were tested with Pearson's correlations based on their raw continuous values. They were then assessed with a linear, or multiple, regression analysis. The aim in this analysis was to produce a regression equation that could be used to predict juvenile age at death from bone histology.

5.2 Descriptive Statistics

A total of 83 juvenile skeletons were analysed as part of this study. The sample was split into four age categories. The infant class is aged 0-1.9 years, the early child class is aged 2-7.9 years, the late child class is 8-13.9 years, and the adolescent class is 14-18.9 years. The skeletons were also split into three robusticity categories based on their robusticity indices. The third of the skeletons with the smallest robusticity indices were placed in the low robusticity category, the third with the middle robusticity indices were placed in the mid robusticity category, and the third with the largest robusticity indices were placed in the high robusticity category.

	Infant (0-1 yrs)	Early Child (2-7 yrs)	Late Child (8-13 yrs)	Adolescent (14-18 yrs)	Total
Low Robusticity	0	5	12	9	26
Mid Robusticity	0	12	12	3	27
High Robusticity	5	18	3	0	26
Total	5	39 *	27	12	83 *

* 4 individuals in the early child class did not have a robusticity. The total sample size = 83.

Table 5.1 Age and robusticity frequencies

The breakdown of sample sizes for the groupings can be seen in **table 5.1**. The largest age group was the early childhood age class (N=39) at 47% of the total sample size. The smallest age class was the infants (N=5) at only 6% of the total sample size. In the infant class there were no individuals who had a low or mid level of robusticity. While in the adolescent class there were no individuals who had a high level of robusticity. Also, 51% of the early child class was also in the high robusticity group but only 11% of the late child class was. It would appear that robusticity of the humerus decreases with age. This is most likely caused by large increases in length during the juvenile growth period and the comparatively much smaller increase in width in the same period.

Table 5.2 shows the mean values for each variable subdivided by age class. It can be seen that the mean height increases for each subsequent age class. This is the expected pattern, as children grow taller as they get older until they obtain their adult height. As such this provides an indication that the data is accurate. From the mean values it would appear that the primary osteon population density decreases with age and that the secondary osteon population density increases with age. It also seems that the area of the secondary osteons increases with age. The mean values suggest that the secondary osteons and their canals get more irregular with increasing age. The minimum diameters

of the osteons and their canals decrease, while the maximum diameters of the osteons and their canals increase. This would mean that the secondary osteons become less circular with age.

Table 5.3 shows the mean values for each variable split by robusticity group. Only the early childhood age class, the largest sample size for one age class, was used. The mean values show that less robust children are taller. However, this is likely to be caused by the taller children having longer and therefore less robust limbs. There appears to be a link between robusticity and secondary osteon population density. More robust children had fewer secondary osteons than less robust-age matched children. Secondary osteon area may also decrease with increasing robusticity.

Variable		Infant	Early Child	Late Child	Adolescent
Robusticity	**Mean**	15.912	14.700	13.301	12.529
	SD	0.666	1.600	1.305	1.153
Height	**Mean**	74.300	96.154	128.332	152.250
	SD	3.291	12.236	9.237	9.531
Osteon Population Density	**Mean**	5.984	5.025	7.209	7.701
	SD	2.157	1.657	1.865	1.375
Primary Osteon Population Density	**Mean**	5.984	4.039	3.146	0.701
	SD	2.157	1.364	1.409	1.060
Secondary Osteon Population Density	**Mean**	0.000	0.814	4.316	7.032
	SD	0.000	1.069	1.485	1.323
Primary Canal Area	**Mean**	1078.340	1180.880	1179.450	1004.664
	SD	207.891	242.975	248.983	262.374
Primary Canal Minimum Diameter	**Mean**	17.496	18.933	19.509	23.540
	SD	4.448	3.053	4.473	5.063
Primary Canal Maximum Diameter	**Mean**	67.800	68.961	83.484	47.252
	SD	14.865	14.525	72.245	4.887
Secondary Osteon Area	**Mean**		30203.787	33955.210	41613.759
	SD		11849.382	9561.122	10171.843
Secondary Osteon Minimum Diameter	**Mean**		132.234	122.390	121.498
	SD		22.738	27.128	19.414
Secondary Osteon Maximum Diameter	**Mean**		252.368	319.588	376.248
	SD		79.023	67.067	55.384
Secondary Canal Area	**Mean**		1940.094	1791.388	1832.3342
	SD		812.501	400.741	584.692
Secondary Canal Minimum Diameter	**Mean**		28.016	23.080	18.744
	SD		9.441	4.133	2.161
Secondary Canal Maximum Diameter	**Mean**		71.005	83.328	97.498
	SD		23.1220	16.465	20.469
Number of Lacunae	**Mean**		72.140	62.560	53.330
	SD		22.229	17.487	6.713

Table 5.2 Mean values of each variable subdivided according to age group.

Variable		Early Childhood Age Group		
		Low Robusticity	Mid Robusticity	High Robusticity
Height	**Mean**	107.400	94.755	91.667
	SD	0.141	9.694	12.386
Osteon Population Density	**Mean**	6.336	5.775	4.606
	SD	1.528	2.044	1.420
Primary Osteon Population Density	**Mean**	3.840	3.989	4.065
	SD	1.074	1.692	1.226
Secondary Osteon Population Density	**Mean**	2.500	1.787	0.541
	SD	1.433	2.107	1.047
Primary Canal Area	**Mean**	1241.614	1138.349	1074.698
	SD	176.877	239.540	227.608
Primary Canal Minimum Diameter	**Mean**	18.732	18.185	19.540
	SD	2.620	2.544	3.374
Primary Canal Maximum Diameter	**Mean**	80.854	80.186	61.677
	SD	16.138	52.759	10.680
Secondary Osteon Area	**Mean**	37634.67	31655.80	26379.75
	SD	15350.75	8853.412	5635.548
Secondary Osteon Minimum Diameter	**Mean**	145.878	130.938	123.814
	SD	25.491	23.140	24.244
Secondary Osteon Maximum Diameter	**Mean**	295.490	284.571	224.245
	SD	101.230	69.805	57.439
Secondary Canal Area	**Mean**	1819.466	2008.306	1755.070
	SD	705.021	765.832	799.884
Secondary Canal Minimum Diameter	**Mean**	28.264	27.609	27.769
	SD	5.937	9.850	11.068
Secondary Canal Maximum Diameter	**Mean**	75.178	77.795	65.050
	SD	24.842	21.491	15.440
Number of Lacunae	**Mean**	84.500	69.500	60.00
	SD	16.263	8.062	24.062

Table 5.3 Mean values for each robusticity group for the early childhood age group.

5.3 Comparisons Between the Age Classes

5.3.1 Frequency Variables

Osteon population density

A one way ANOVA was used to compare osteon population density between the age groups. There was statistically significant difference between the groups ($F(3,79) = 12.207$, $p < 0.000$). A Tukey post-hoc test revealed that the osteon population density of the early childhood age class (mean = 5.025) was significantly less compared to the density (mean = 7.209) of the late childhood age class ($p > 0.000$).

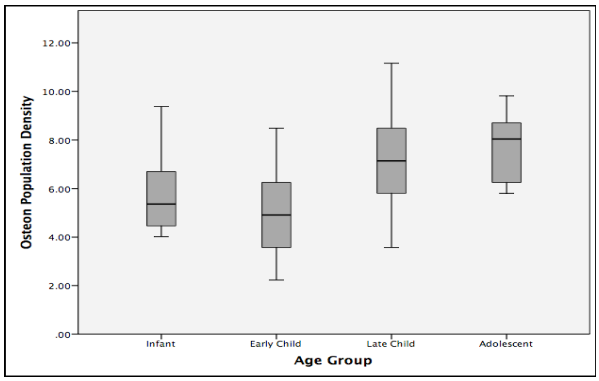

Graph 5.1 Box plot of age with osteon population density.

Primary osteon population density

Primary osteon population density differed significantly between the age groups ($F(3,79) = 27.945$, $p < 0.001$). A Tukey post-hoc test revealed a significantly higher frequency of primary osteons in the infant class (mean = 5.984), compared to the early childhood age class (mean = 4.039; $p = 0.040$), the late childhood age class (mean = 3.146; $p < 0.001$), and the adolescent class (mean = 0.701; $p = 0.040$). Significant differences also occurred between the early and late childhood age classes ($p = 0.001$), between the early childhood and adolescent classes ($p < 0.001$), and between the late childhood and adolescent classes ($p < 0.001$).

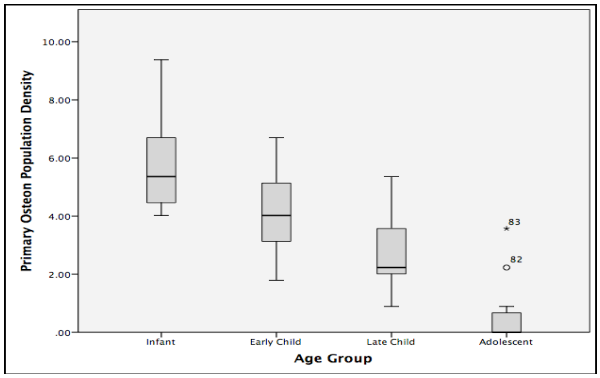

Graph 5.2 Box plot of age with primary osteon population density.

Secondary osteon population density

A one way ANOVA showed that there was a statistically significant when the secondary osteon population density was compared between the age groups ($F(3,79) = 103.152$, $p < .001$). Employing the Tukey post-hoc test, significant differences were found between the lower frequencies of the infant class (mean = 0.000) and the late childhood class (mean = 4.316; $p < 0.001$), and the adolescent class (mean = 7.032; $p < 0.001$). The secondary osteon population density was also significantly lower in early childhood (mean = 0.814) compared to the late childhood class ($p < 0.001$), and to the adolescent class ($p < 0.001$). It was also lower in the late child group than in the adolescent class ($p < .0005$).

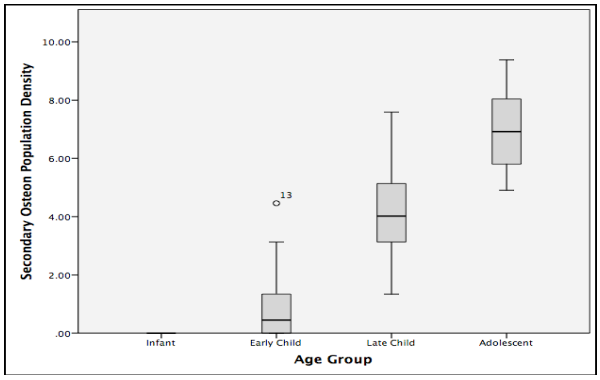

Graph 5.3 Box plot of age with secondary osteon population density.

5.3.2 Summary

Age has a significant effect on the density of all types of osteons. However, it affects each type of osteon in a different manner. The primary osteon population density decreases with increasing age. The infant class has significantly more primary osteons than the early child class, which in turn has significantly more than the late child class, which also has significantly more primary osteons than the adolescent class. The secondary osteon population density exhibits the opposite pattern. The early child class has significantly less secondary osteons than the late child class, which has significantly less than the adolescent class.

5.3.3 Size Variables

Secondary osteon area

A one way ANOVA showed a statistically significant difference in the size of secondary osteon areas when compared across the four age groups ($F(2,61) = 4.676$, $p = 0.013$). The Tukey post-hoc test showed that the size of secondary osteons in the early childhood age class (mean=30203.787) was significantly smaller compared to the adolescents (mean=41613.759; p=0.009).

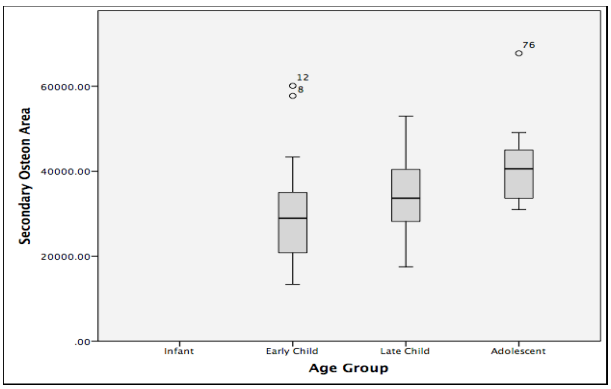

Graph 5.4 Box plot of age with secondary osteon area.

Secondary osteon maximum diameter

A one way ANOVA showed that the secondary osteon maximum diameter varied significantly with age ($F(2,60) = 13.571$, $p < 0.001$). The Tukey post-hoc test showed that the maximum diameter was significantly smaller in the early child class (mean = 252.368) than the late childhood class (mean = 319.588; $p = 0.003$), or the adolescent class (mean = 376.248; $p < 0.001$).

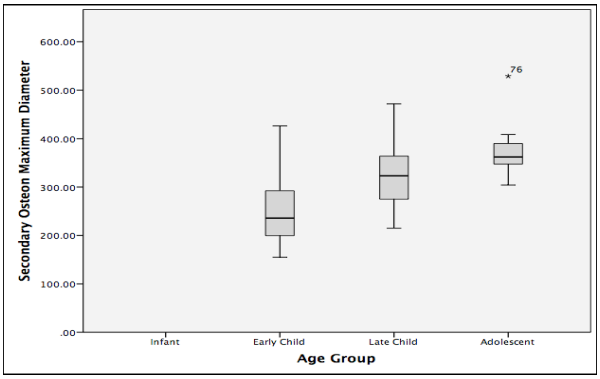

Graph 5.5 Box plot of age with secondary osteon maximum diameter.

Secondary osteon canal minimum diameter

A one way ANOVA was used to compare the secondary osteon canal minimum diameter between the age groups. There was statistically significant difference between the groups ($F(2,60) = 8.725$, $p < 0.001$). The Tukey post-hoc test showed that the minimum diameter was larger in the early child class (mean = 28.016) than the late child class (mean = 23.080; $p = 0.024$), and the adolescent class (mean = 18.744; $p = 0.003$).

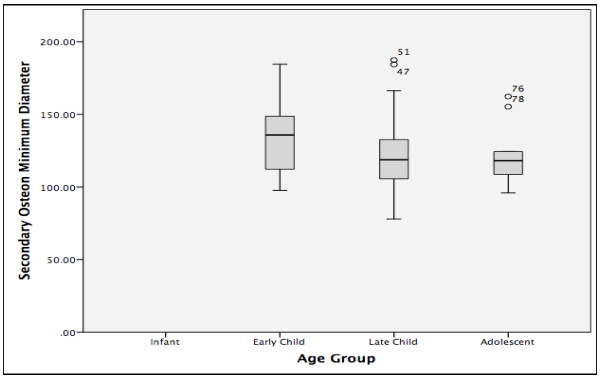

Graph 5.6 Box plot of age with secondary osteon minimum diameter.

Secondary osteon canal maximum diameter

A one way ANOVA showed that there was a statistically significant difference between the age groups in the secondary osteon canal maximum diameter ($F(2,60) = 7.268$, $p = 0.001$). A Tukey post-hoc test revealed that the early child class (mean = 71.005) had significantly smaller maximum diameters than the adolescent class (mean = 97.498; $p = 0.001$).

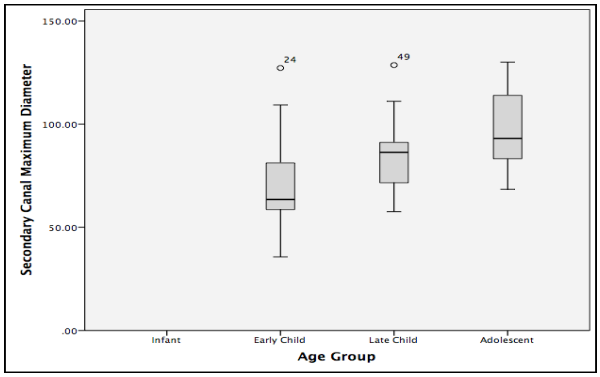

Graph 5.7 Box plot of age with secondary osteon canal maximum diameter.

5.3.4 Summary

Age significantly affects the dimensions of secondary osteons but not primary osteons. The area of secondary osteons, and secondary osteon maximum diameter, differ significantly between the early childhood and the adolescent classes. The differences between the intervening age categories are mostly non significant. The area of the secondary osteons increases with age, as does the maximum diameter. This means that the secondary osteons become less circular with age.

Additionally, the dimensions of the secondary osteon vascular canals are significantly affected by age, unlike primary osteon vascular canals. There are significant differences between the early child class and the adolescent class for the secondary osteon canal minimum and maximum diameters. The differences between the intervening age classes

are non significant. The secondary osteon canal minimum diameter decreases with age, while the maximum diameter increases with age. This means that the secondary osteon canals become less circular with age.

5.4 Comparisons Between the Robusticity Groups

5.4.1 Frequency Variables

Secondary osteon population density

A one way ANOVA showed that the secondary osteon population density varied between the robusticity categories for age matched children ($F(2,32) = 12.732$, $p < 0.001$). A Tukey post-hoc test revealed that the secondary osteon population density of the low robusticity category (mean = 2.500) was significantly more compared to the density (mean = 1.787) of the mid robusticity category ($p = 0.005$), and the density (mean = 0.541) of the high robusticity category ($p < 0.001$).

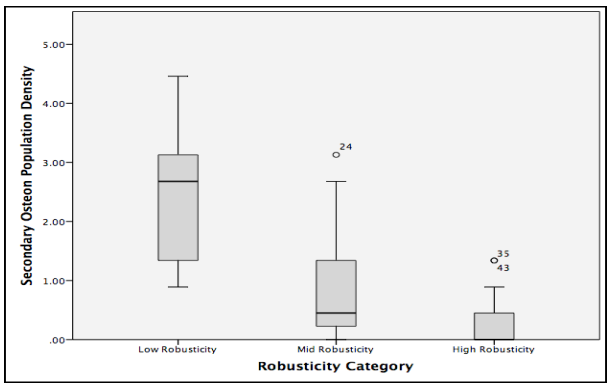

Graph 5.8 Box plot of robusticity with secondary osteon population density.

5.4.2 Summary

For the early childhood age group (aged 2-7 years) the robusticity of the humerus exerts a significant influence on the population density of secondary osteons. Those individuals in the low robusticity group had a higher secondary osteon population density than those in the high robusticity group.

5.5 Correlations with Age

5.5.1 Frequency Variables

Osteon population density

A spearman's r_s indicated that there was a significant positive correlation between age category and osteon population density ($r_s = 0.514$, $N = 83$, $p < 0.001$). It is a moderate correlation, with 26.4% of the variation explained.

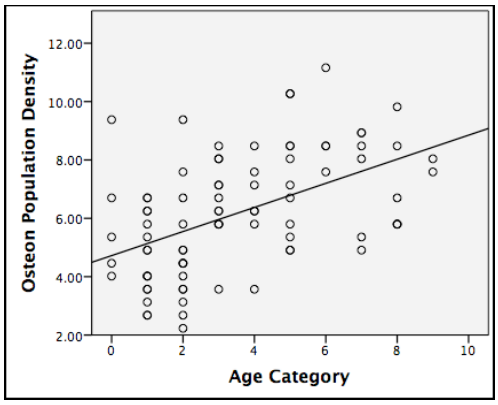

Graph 5.9 Correlation between age and osteon population density.

Primary osteon population density

A spearman's r_s indicated that there was a significant negative correlation between age category and primary osteon population density (r_s = -0.672, N = 83, p < 0.001, two tailed). It is a moderate correlation with 45.2% of the variation explained.

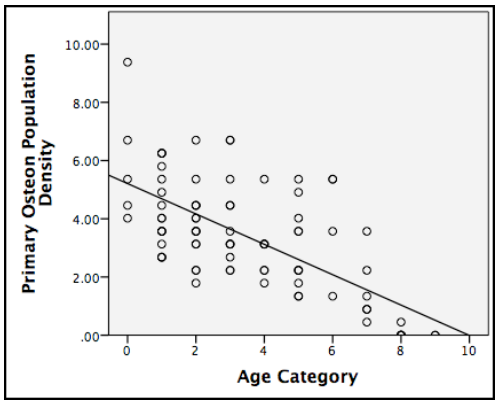

Graph 5.10 Correlation between age and primary osteon population density.

Secondary osteon population density

A spearman's r_s indicated that there was a significant positive correlation between age category and the secondary osteon population density (r_s = 0.878, N = 83, p < 0.001). It is a strong correlation, with 77.1% of the variation explained.

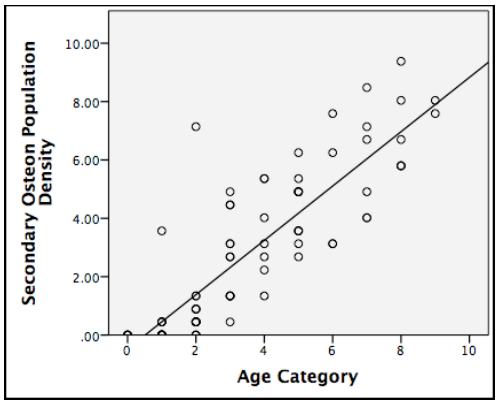

Graph 5.11 Correlation between age and secondary osteon population density.

5.5.2 Summary

Age category has a significant affect on the density of all types of osteons. However, it affects each type of osteon in a different manner. There is a positive correlation between age and total osteon population density in the humerus. Age and secondary osteon population density also exhibit a positive correlation. There is an overall increase in the density of osteons with age, and this is caused by a large increase in the density of the secondary osteons. In contrast, age is negatively correlated with primary osteon population density. There are fewer primary osteons present as an individual ages.

5.5.3 Size Variables

Secondary osteon area

A spearman's r_s indicated that there was a significant positive correlation between age and secondary osteon area (r_s= 0.392, N = 64, p = 0.001). It is a weak correlation with 15.4% of the variation explained.

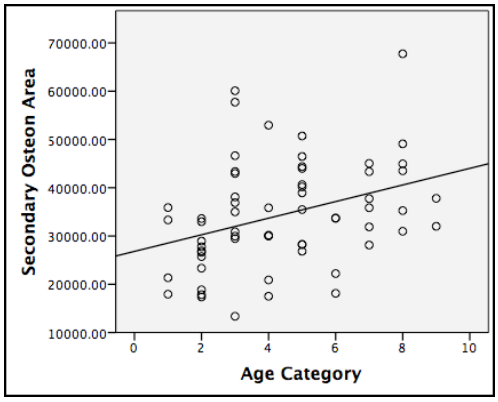

Graph 5.12 Correlation between age and secondary osteon area.

Secondary osteon maximum diameter

A spearman's r_s indicated that there was a significant positive correlation between age and secondary osteon maximum diameter (r_s = 0.559, N = 63, p < 0.001). It is a moderate correlation with 31.2% of the variation explained.

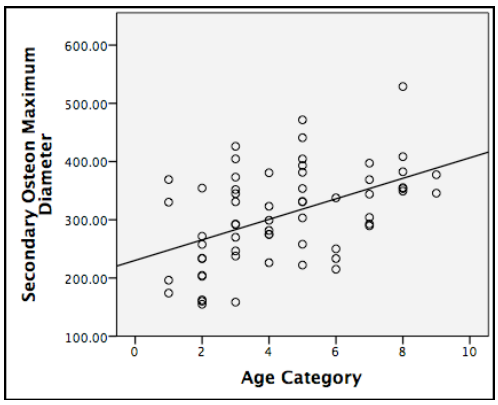

Graph 5.13 Correlation between age and secondary osteon maximum diameter.

Secondary osteon canal minimum diameter

A spearman's r_s indicated that there was a significant negative correlation between age and secondary osteon canal minimum diameter (r_s = -0.475, N = 63, p < 0.001). It is a weak correlation with 22.6% of the variation explained.

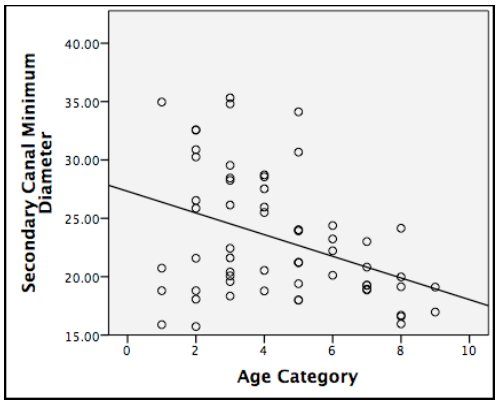

Graph 5.14 Correlation between age and secondary osteon canal minimum diameter.

Secondary osteon canal maximum diameter

A spearman's r_s indicated that there was a significant positive correlation between age and robusticity ($r_s = 0.439$, $N = 63$, $p < 0.001$). It is a weak correlation with 19.3% of the variation explained.

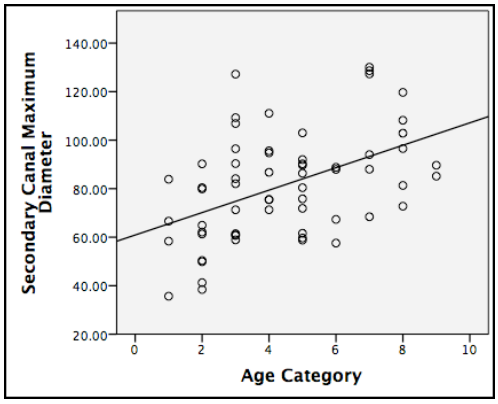

Graph 5.15 Correlation between age and secondary osteon canal maximum diameter.

5.5.4 Summary

Age category significantly affects the dimensions of secondary osteons, but not primary osteons. The area of the secondary osteons is positively correlated with age. As such the area of secondary osteon area increases as an individual gets older. This increase in area is caused by an increase in the maximum diameter of the secondary osteons and not by any accompanying increase in the minimum diameter. The secondary osteon maximum diameter exhibits a positive correlation with age. The secondary osteon minimum diameter shows no significant correlation with age.

Additionally, only the dimensions of the secondary osteon vascular canals are affected by age. The dimensions of the primary osteon vascular canals are not significantly affected by age. The secondary osteon canal maximum diameter is positively correlated with age, as such the canal maximum diameter gets larger with age. While the

secondary osteon canal minimum diameter is negatively correlated with age, as such the canal minimum diameter gets smaller as age increases.

5.6 Correlations with Robusticity

5.6.1 Frequency Variables

Secondary osteon population density

A spearman's r_s indicated that there was a significant negative correlation between robusticity and secondary osteon population density (r_s = -0.642, N = 35, p < 0.001). It is a strong correlation with 41.2% of the variation explained.

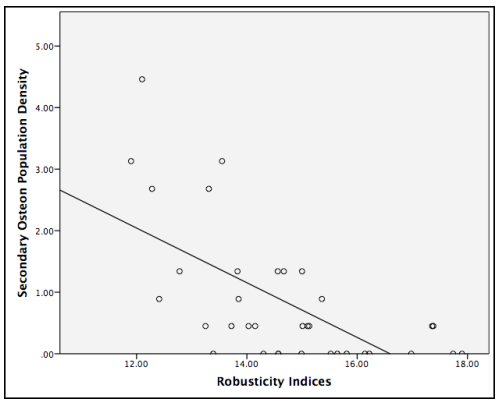

Graph 5.16 Correlation between robusticity and secondary osteon population density.

5.6.2 Summary

For the early child class (aged 2-7.9 years) the robusticity of the humerus has a significant affect on the population density of the secondary osteons. There is a negative association between robusticity and secondary osteon population density. As such, those individuals in the low robusticity group had a higher secondary osteon population density than those in the high robusticity group.

5.7 Regression Analysis

5.7.1 Linear Regression

Primary osteon population density and secondary osteon population density were the two variables that were most strongly correlated with age. The two variables were separated from the others and the analysis was repeated using a Pearson's correlation on the raw data, rather than the ranked data. The Pearson's correlations revealed that age and primary osteon population density were negatively and significantly correlated (r = -0.693, N = 83, p < 0.001). Age and secondary osteon population density were positively and significantly correlated (r = 0.922, N = 83, p < 0.001). These relationships are shown in Graph 5.17. The two variables were selected for a linear regression analysis, to construct an equation that would allow age to be estimated from primary and secondary osteon population density.

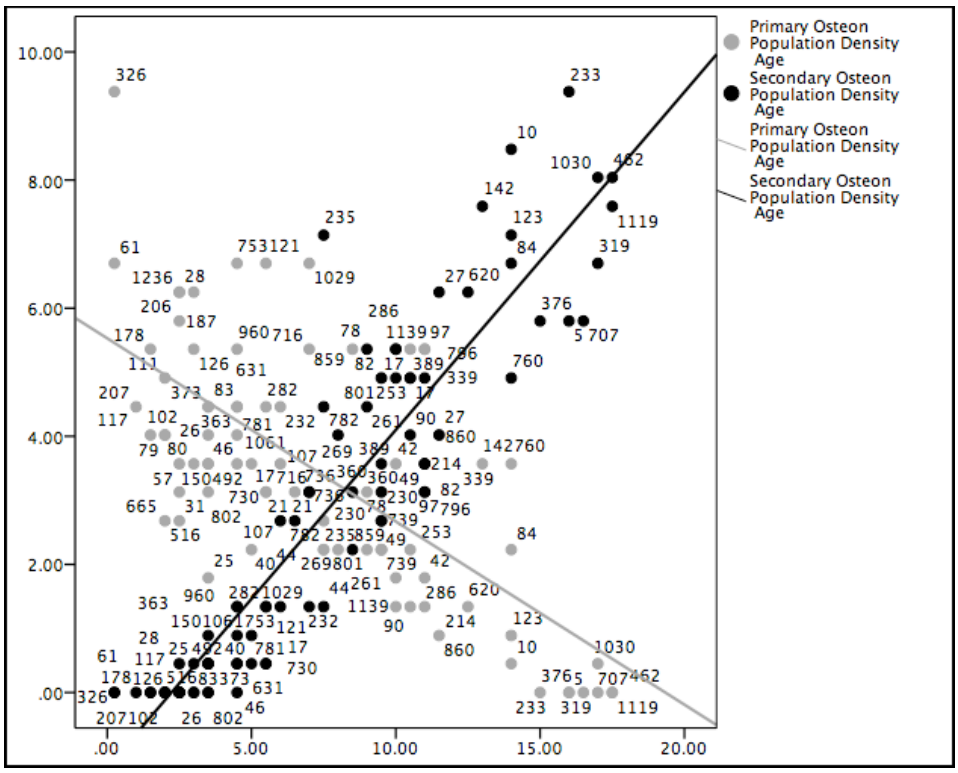

Graph 5.17 Correlation between age and primary and secondary osteon population density.

Primary osteon population density was used in a linear regression analysis to predict age at death. Using the enter method, a significant model emerged, whereby F (1,81) = 75.048, $p < 0.001$. The model explains 48% of the variance ($R^2 = 0.481$, Adjusted $R^2 = 0.475$). **Table 5.4** gives information for the predictor variable entered into the model. Primary osteon population density was a significant predictor of age.

Variable	B	SE B	β	p
Constant	13.215	0.750		< 0.001
Primary osteon population density	-1.680	0.190	-0.690	< 0.001

Table 5.4 Regression table for primary osteon population density.

Secondary osteon population density was used in a linear regression analysis to predict age at death. Using the enter method, a significant model emerged, F (1,81) = 461.741, $p < 0.001$. The model explains 85% of the variance ($R^2 = 0.851$, Adjusted $R^2 = 0.849$). **Table 5.5** gives information for the predictor variable entered into the model. Secondary osteon population density was a significant predictor of age.

Variable	B	SE B	β	p
Constant	3.020	0.290		< 0.001
Secondary osteon population density	1.613	0.080	0.920	< 0.001

Table 5.5 Regression table for secondary osteon population density.

Both variables produced models that could be used to predict juvenile age-at-death. However, secondary osteon population density was a better predictor of age than primary osteon population density was. Using secondary osteon population density as the predictor variable explained more of variation than by using the primary osteon population density. By combining the two variables in a multiple regression it could be possible to produce a stronger model.

5.7.2 Multiple Regression

The two variables, primary osteon population density and secondary osteon population density, were combined in a multiple linear regression analysis. The aim was to determine if a combination of variables would have a stronger predictive power for age at death than either variable did separately.

Primary osteon population density and secondary osteon population density were used in a multiple linear regression analysis to predict juvenile age-at-death. The predictor variables are negatively correlated (r = -.655, N = 83, $p < 0.001$). Using the enter method, a significant model emerged, whereby F (2,80) = 255.820, $p < 0.001$. The model explains 86.1% of the variance (R^2 = 0.865, Adjusted R^2 = 0.861). **Table 5.6** gives information for the predictor variables entered into the model. Both primary osteon population density and secondary osteon population density were significant predictors of age.

Variable	B	SE B	β	p
Constant	4.810	0.680		< 0.001
Primary osteon population density	-0.380	0.130	-0.160	0.005
Secondary osteon population density	1.430	0.100	0.820	< 0.001

Table 5.6 Regression table for primary and secondary osteon population density.

Regression equation:

Age (yr) = 4.806 + (-.38 x POPD) + (1.43 x SOPD)

This equation will predict the age at death for juveniles based on the primary osteon population density and the secondary osteon population density of the midshaft humerus.

5.7.3 Summary

Both primary osteon population density and secondary osteon population density were significant predictors of age. When combined in a multiple regression analyses they produced a model that could predict age at death. The model is a strong predictor of age at death and explains 86.1% of the variance in the estimate.

By using the equation that the model produced it should be possible to predict the age at death of an individual from a fragment of the humerus, based on the primary osteon population density and the secondary osteon population density.

CHAPTER 6.

DISCUSSION

6.1 Introduction

This chapter will begin with a discussion of the results of the study. This portion will be split into three parts according to the three aims. Each will contain an explanation of the results and a comparison to the published literature. The first part will cover the results that are associated with the histological changes within the humerus, as an individual ages. The next part will cover the results that are associated with how the histology varies according to robusticity. The last part will cover the estimation of age from bone histology.

Every study is affected to a greater or lesser extent by limitations. The limitations that have affected this study will be discussed in the next section of this chapter. These include sampling issues, such as the unknown chronological age of the sample, and issues caused by the location that the histological section was removed from. There were also some important limitations to the methodology, including both macroscopic and microscopic techniques. This section will also explain the steps that were taken to limit the impact of these limitations.

The chapter will conclude by suggesting improvements and extensions to this study for future investigation. Future studies would ideally expand upon the results of this study and test the reliability and accuracy of the proposed age estimation method. There are

examples of how to improve the reliability of the techniques, and how to test the regression equation for predicting juvenile age at death.

6.2 Age Variation

Age was found to be significantly correlated with the number of primary osteons. The number, and therefore density, of primary osteons decreases as age increases. Although the number of primary osteons changes with age there is no significant change in the size or shape of the primary osteons over time. Further to this, there are no significant changes to the size and shape of the vascular canals of the primary osteons as age increases.

Primary osteons are formed by modelling activity. The size and morphology of the primary osteons does not change as age increases because they are formed early in the growth of the bone. Primary osteons make up primary bone tissue and so only form when new bone is formed. It would appear that there are fewer new primary osteons formed after infancy, and hardly any formed once the bone reaches its adult size. One result, the size of primary osteon canal, does not follow expectations from previous research. Experimental research in non-human animals has demonstrated that primary vascular canals are in-filled by bone deposition (Castanet et al., 2000; Starck and Chinsamy, 2002; Cubo et al., 2008). Based on this research it was expected that primary osteon canal area would decrease with advancing age. One reason that this was not found here might be differences in the developmental trajectories. It is possible that there is more variation in canal size within the age classes rather than between them.

The number of secondary osteons was found to correlate with age. The number, and therefore density, of secondary osteons increases as age increases. The size of the secondary osteons is also correlated with age. The area of the secondary osteons increases over time. This increase in size is the result of an increase in the length of the secondary osteon maximum diameter. The secondary osteon minimum diameter does not change significantly. This has the effect of producing less circular and more irregular secondary osteons as the bone ages. The vascular canal of the secondary osteon also becomes more irregular with increasing age, although, there is no overall change in size in the canal with age. The canal minimum diameter gets smaller, while the maximum diameter gets larger over time. The result is an increasing number of secondary osteons that become larger and less circular with less circular canals as a juvenile ages.

Secondary osteons are formed by remodelling activity. This remodelling begins in early childhood and continues until death (Stout and Crowder, 2012). The original primary bone is gradually replaced by the secondary osteons until there is no primary bone remaining. This results in an increase in the number and density of secondary osteons with in the bone as it ages. The correlation between increasing secondary osteon population density and advancing age is well documented. Many studies have produced age at death estimation methods for adult remains based on this correlation (Kerley, 1965; Kerley and Ubelaker, 1978; Thompson, 1979; Thompson and Galvin, 1983; Han et al., 2009).

The size of secondary osteons is determined by the amount of bone that is removed by osteoclasts (Qui et al., 2003). Thus, assuming a constant rate of bone deposition, the

diameter of the osteon will indicate the activity level of the BMUs. Larger osteons could indicate a slower rate of BMU activity because it takes longer to remove a large area of bone and deposit more lamellae (Pfeiffer et al., 2006). Given that this study found that secondary osteon area increases with age it could be that BMU activity decreases with age. The size has also been linked to the extent on the strain on the bone. Smaller osteons are correlated with larger strains (van Oers et al., 2008). As such it is also possible that the humerus is subject to less strain as the juvenile period progresses. This could be a result of the increased modelling during this period strengthening the bone and reducing the strain.

This study found that the maximum diameter of the secondary osteon increases with increasing age, while the minimum diameter has no significant change. This results in a reduction in the circularity of secondary osteons over time as age increases. This is accompanied by a reduction of the circularity of the vascular canal. In adults the opposite pattern occurs. Secondary osteons have been found to become more circular with increasing age (Currey, 1964; Britz et al., 2009). There are several possible explanations for this pattern and its reversal. One possibility is that drifting osteons are remodelled by more circular osteons. Another is that the osteons are sectioned at an oblique angle in juveniles and the orientation changes with age.

It is possible that this pattern is caused by an accumulation of drifting osteons in the cortex during the juvenile period. Drifting osteons are defined as "Haversian systems in which there is continuous resorption on one side and continuous formation on the other" (Robling and Stout, 1999:193). This forms an osteon that appears to have a tail (Stout and Crowder, 2012). The tail indicates the direction of the drift. The precise mechanism

for the formation of drifting osteons is not clear, but they are believed to be the result of a complex loading environment (Robling and Stout, 1999). Drifting osteons are common in juveniles but less common in adults (Stout and Crowder, 2012; Streeter, 2012). The remodelling process would replace the less circular drifting osteons with more circular osteons. Over time the ratio of drifting osteons to circular osteons will decrease, resulting in a more circular average osteon in older individuals.

Alternatively, the shape of the osteon could be related to the type of strain that the bone is exposed to (Hennig at al., 2015). Smaller and more circular osteons have been linked to compressive forces, and larger and less circular osteons have been linked to tensile forces (Skedros et al., 1994). It is possible that the smaller and more circular osteons in later life are a consequence of increased strain (van Oers et al., 2008) caused by increasing porosity and thinning of the cortex (Hennig et al., 2015). This explanation appears to be the more likely of the two because drifting osteons are usually readily identifiable by their tail. Furthermore, the humerus is likely to experience a complex parr tern of loading that varies with age according to the activity level of individuals.

The results of this study support the currently accepted pattern of bone growth (Schuer and Black, 2000). At the start of the development of the humerus a cartilaginous model is calcified and replaced by fast forming woven bone during gestation. Before birth the woven bone is swiftly replaced by primary lamellar bone containing primary osteons. As the humerus expands during early childhood growth, new lamellae and primary osteons are formed at the edges of the diaphysis. The size of the primary osteons is uniform at all ages because they are all formed around blood vessels that have little variation in size. The oldest parts of the primary bone start to be remodelled in early

childhood to prevent fatigue of the bone. This leads to an overall decrease in the number of primary osteons as they are being replaced by secondary osteons. As the humerus diaphysis reaches its adult during adolescence size no new primary bone is created. After this point the major process is remodelling. Secondary osteons keep being formed and eventually secondary bone will replace all of the primary bone. This leads to an overall increase in the number and density of secondary osteons that are present in the bone.

However the morphology of the secondary osteons in the juvenile humerus did not conform to the expected pattern. This indicates that while the density of secondary osteons is strongly related to age, the morphology has a more complicated aetiology. This study did not investigate the mechanical strains that affect the juvenile humerus. This causes some difficulty when attempting to interpret the age related change in the morphology of the secondary osteons. The loading environment that the bone is exposed to during growth is extremely important for the morphology of the bone.

6.3 Robusticity Variation

In an age-matched sample, robusticity was found to have a correlation with the population density of secondary osteons. More robust children had a significantly lower secondary osteon population density than less robust, or gracile, children did. No other histological feature was found to correlate with robusticity, including the size and shape of the secondary osteons.

Primary osteons are formed as a byproduct of bone modelling, in which the area of the cortex increases. While secondary osteons are the primary feature of bone remodelling, in which older bone is resorbed and new bone deposited in its place. This indicates that the robust children in this study underwent greater levels of bone modelling than the gracile children, as evidenced by their larger cortex. Equally, it indicates that the gracile children experienced a greater level of remodelling than the robust children, shown by their increased secondary osteon population density.

There are two ways in which modelling can result in a stronger bone. The first way is to deposit new bone sub-periosteally and reduce the level of endosteal resorption in order to increase the cross-sectional area of the cortex. This makes the bone more robust and better able to resist compressional forces by distributing the force over a larger cross-sectional area. The second way of increasing the strength of the bone also relies on the deposition of new bone sub-periosteally. This increases the bones ability to resist bending and rotational forces. This is a particularly important response to loading in juveniles as this age group has the most metabolically active bone out of any age group (Ruff et al., 1994; Bass et al., 1998; Lieberman and Pearson, 2001; Lieberman et al., 2003). This load induced modelling results in a more robust bone that is more capable of resisting strains than more gracile bones.

Previous research has shown that the magnitude of the strains that bone is exposed to during the juvenile period has a significant impact on the morphology of the bone. Children who exercise regularly have a higher peak bone mass during adolescence than more sedentary children (Bradney et al., 1998). The difference in bone mass has been reported in multiple activities: weight lifting (Fujimura, 1997), gymnastics (Cassell et

al., 1996; Courteix et al., 1998), swimming (Cassell et al., 1996), tennis (Kannus et al., 1995), and jumping (Fuchs et al., 2001; Gunter et al., 2012). These all lend support to the theory that strains caused by activity lead to greater levels of modelling. The loading environment during the juvenile period is particularly important for the architecture of the adult bone as this is the most active period for both bone modelling and remodelling (Pearson and Lieberman, 2004). The bone mass that is accrued during the juvenile period is maintained for life (Strauss et al., 2001; Kimm et al., 2002; Baxter-Jones et al., 2008; Janz et al., 2010; Francis et al., 2014). An individual that has robust bones as a juvenile will usually have more robust bones throughout adulthood and into old age. Whereas, an individual with gracile bones as a juvenile will usually continue to have gracile bones throughout life, and may be more at risk for osteoporosis in later life (Ferrari et al., 1998; Dertina et al., 1998, Nikander et al., 2010).

This work provides one explanation why the more robust children in this study were found to have lower secondary osteon population densities than the more gracile children. The robust children may have been more active during life, leading to more habitual stress on their bones, which caused strain induced modelling to strengthen the bone. Their larger cortex was the result this process. A different explanation is needed to explain why the gracile children exhibited signs of remodelling.

There are several theories that seek to explain the ultimate causes of bone remodelling. All of the theories agree that histomorphology changes in response to the loading environment of the bone in order to prevent the fatigue and possible failure of the bone. However, there is currently no agreement about the mechanism that causes remodelling.

There are two main competing theories. These are the mechanostat hypothesis and the optimisation theory.

The mechanostat hypothesis explains that strains above a particular threshold will stimulate modelling but inhibit remodelling, while strains below a lower threshold will inhibit modelling and stimulate remodelling (Frost, 1986, 1987, 1990). Strains that are between the two thresholds will not stimulate either modelling or remodelling. However, few studies completely support this hypothesis. While high strains often cause bone modelling and low strains are correlated with bone resorption (Martin et al., 1998) high strains have also been found to stimulate bone remodelling (Goodship and Cunningham, 2001; Lieberman et al., 2003).

Optimisation theory predicts how different bones in the skeleton respond to loading (Lieberman and Crompton, 1998; Lieberman et al., 2001; Lieberman et al., 2003). It predicts that if bones optimise strength relative to the cost of growing new bone then the proportion of modelling versus remodelling in response to loading will vary across the skeleton and at different times in relation to a cost/benefit ratio (Pearson and Lieberman, 2004). The most important benefit of modelling is that the added mass will increase the strength of the bone, which is particularly important in response to bending. However, the cost of adding mass to the limbs is that the energy needed to propel the limb during locomotion will be higher (Marsh et al., 2004). The costs and benefits of remodelling may include the replacement of damaged and fatigued bone, an increase in elasticity, and reduced micro-crack propagation (Martin et al., 1998; Schaffler et al., 1990; Currey, 2002). A known cost of remodelling is a higher long-term metabolic cost because further remodelling will be required in the future (Martin, 1995). The

modelling response to strains declines with age and so the rate of remodelling increases with age (Lieberman et al., 2003).

Without experimental data it is not clear which of the two theories best explains the pattern that was found here. The mechanostat theory fails to explain the complexity of the interaction between the loading environment and bone modelling and remodelling. Equally the optimisation theory does not fully explain why some juveniles appear to be bone modellers while others appear to favour remodelling in the same bone at comparative ages. Given that robusticity is a proxy for activity level, it is possible that less active children are not exposed to habitual strains resulting in less modelling. The gracile bones are less able to withstand stressors than robust bones. Consequently, they may respond to acute strains with remodelling to make up for the lack of strength. If this explanation is accurate then it would indicate that the duration of the strain is as important as the intensity of the strain for irritating either modelling or remodelling. This is one possible explanation. Further research, preferably experimental in nature, is needed to fully understand the nature of secondary osteon initiation, formation, and growth.

This study found that robust children have a lower secondary osteon population density than gracile children. It is possible that the larger overall bone size of the more robust children was able to respond well to the stressors on the bone. Whereas the narrower bone of the more gracile children was less able to respond well to the stressors of the bone, and as a consequence remodelled to increase the strength of the bone. This study provides evidence that the formation of secondary osteons is not solely reliant on

advancing age. The low levels of activity during childhood can result in secondary osteon formation to make up for the lack of strength in the bone.

6.4 Age-at-Death Estimation

Both primary osteon population density and secondary osteon population density were found to have a significant correlation with age at death. Primary osteon population density had a strong negative correlation with age. Secondary osteon population density had a strong positive correlation with age. As such both the primary and secondary osteon population densities of the humerus can be significant predictors of age at death in juveniles. When these variables were combined in a multiple regression analyse they produced a model that could predict age at death. The model is a strong predictor of age at death and explains 86.1% of the variance in the estimate. By using the equation that the model produced it should be possible to predict the age at death of a juvenile from a fragment of the humerus, based on the primary osteon population density and the secondary osteon population density.

Most histologically based age-at-death estimations have only covered adult remains, or bone remodelling, until this study. There has been one method to estimate juvenile age at death from bone histology previously. Streeter (2005, 2010) examined the rib histology of 72 juveniles with a known age at death. A pattern of microstructural changes within the rib was described. From this, four distinct phases were created. The first phase covers perinatal remains until the beginning of the fifth year, in which woven bone is replaced by primary bone. The second phase covers children aged five to nine,

whose bone was characterised by drifting osteons. The third phase is the largest, ages ten to seventeen, and is described as a mix of drifting osteons and primary osteons. The last phase includes ages eighteen to twenty one, and is characterised by an increase in the number of secondary osteons and a decrease in the number of primary osteons.

The pattern of histological changes described by Streeter (2005) corresponds well with the findings of this study with the exception of the drifting osteons. However, there are a few limitations to Streeter's method. The first is that the method is based on a qualitative examination of the histology. Qualitative analysis is more affected by inter observer variation than a quantitative analysis is. Secondly, the age categories are very broad for juvenile remains. Traditional age-at-death estimation techniques are often able to estimate juvenile age at death to a range of a couple of years. Additionally, this study found that the trends in juvenile bone were continuous and could not be split into age groups as in Streeter's method. When tested, Streeter's method was found to provide a poor estimate of age (Agnew et al., 2007). Agnew et al. (2007) tested the method on medieval remains from Poland that were aged using standard techniques and found only a 38% agreement between the two estimates.

The age at death estimation method produced in this study relies on a quantitative analysis of the bone. This should reduce the inter observer error that is associated with the method. Additionally, the regression equation produces a narrower estimate of age with 86.1% accuracy. However, this method has not been tested on other populations. Extrinsic factors that could affect bone microstructure are likely to vary between populations. It is possible that this equation is population specific, so it will need testing on populations from different geographical areas and different times. Further to this, the

equation may not be applicable to other bones in the body, due to localised factors that affect individual bone growth. This histological method for estimating age at death in juveniles can be applied to remains from medieval Canterbury. Further testing is needed to assess the extent to which this method can be applied to other populations.

6.5 Limitations

There are several limitations in this study, relating to the sampling, methodology, and analysis. The first limitation of the sample is that the true age at death is not known. This is a limitation that is common to most osteological studies that have a sample from an archaeological population. However, the currently accepted methods of estimating age-at-death are much more precise for juveniles than they are for adults.

Another limitation is that only one bone was tested. It is possible that other bones may yield different results. Different bones in the body have different bone turnover rates, which could affect the appearance of the bone microstructure (Stout, 1995; Pearson and Lieberman, 2004). Equally, bone growth is affected by extrinsic factors that may have different effects on different parts of the body.

The next limitation of the current study is that it only tested one population. Bone growth is a dynamic process that is affected by a range of extrinsic and intrinsic factors. The intrinsic factors will vary within populations, while many of the extrinsic factors are more likely to vary between populations. For instance the diet of a land locked population may be more plant based than a coastal population with access to marine

protein. Furthermore, populations that occupy the same geographical space at different times may have very different activity profiles. These types of differences could have an affect on the appearance of the bone microstructure. Thus it is important to test whether the results of this study, and the age at death estimation equation that is based on them, are specific to mediaeval Canterbury. It is possible that bone microstructure does vary temporally and spatially.

6.6 Future Studies

In order to obtain a better appreciation of how bone microstructure varies with age there are several ways to expand this study further. One future study could investigate whether bone microstructure varies between different bones in the body. Some bones have higher bone turnover rates than others, so it is possible that different bones have different patterns of growth. If so, each bone would need a different regression equation to predict the age at death of an individual. Depending on the results of this study it may be possible to produce a regression equation that can be used for any bone.

It is currently unclear whether the regression equation that was produced in this study can be applied to other populations. Only individuals from the medieval period of Kent were included in this study. Due to the nature of the sample the regression equation may be population specific. To rectify this, the regression equation should be tested on individuals from other locations, including other countries if possible, and dating to other time periods. If the predicted age matched the age indicated by standard

osteological techniques then the method is not population specific. If the estimation does not match then it would be necessary to produce a new set of equations.

Another potential future study would be to test whether different taphonomic processes affect the ability to identify primary and secondary osteons. If different postmortem conditions do obscure the histomorphology it would have an impact on the potential forensic applications of this methodology.

CHAPTER 7.

CONCLUSION

As juveniles age, primary lamellar bone is gradually replaced by secondary osteonal bone. This is the currently accepted pattern of juvenile bone growth (Schuer and Black, 2000). At the start of the development a cartilaginous model is calcified and replaced by fast forming woven bone during gestation. Before birth the woven bone is swiftly replaced by primary lamellar bone containing primary osteons. As the humerus grows, new lamellae and primary osteons are formed at the edges of the diaphysis in modelling. The size of the primary osteons is uniform at all ages because they are all formed around blood vessels that have little variation in size. The primary bone is remodelled to prevent fatigue of the bone. This leads to an overall decrease in the number of primary osteons as they are being replaced by secondary osteons. As the humerus diaphysis reaches its adult size no new primary bone is created and the major process is remodelling. Remodelling continues and eventually secondary bone will replace all of the primary bone. This leads to an overall increase in the number and density of secondary osteons.

The correlation of primary bone density and secondary bone density with age was strong. Consequently it was possible to produce a model that could predict juvenile age at death from the primary and secondary osteon population densities of the humerus. The regression equation had an accuracy of 86.1%. This method can be applied in cases where an age at death estimate would not have otherwise been possible due to

incomplete remains. As such it is valuable to biological anthropologists and forensic archaeologists who seek to create a biological profile.

While the density of the primary and secondary bone tissue in the humerus was observed to follow the expected pattern, the morphology of the secondary osteons did not. The age related changes in the morphology of secondary osteons in juveniles exhibit a different pattern to those in adults. In juvenile bone secondary osteons become larger and more irregular as age increases. The opposite has been found in adult bone. Secondary osteons become smaller and more circular with advancing age. The cause of this is not currently known. However, it is possible that the irregular osteons in the juveniles are drifting osteons, which get remodelled during adulthood by more circular osteons. It is also possible that the shape is related to the strain on the bone and that juveniles and adults experience different strains. Additionally, it is not clear at which developmental point the trend reverses.

Secondary osteon formation is not solely linked to advancing age. Robust children have a lower secondary osteon population density than gracile children. Robusticity can be a proxy for activity level. As such it would appear that more active children are exposed to habitual strains that initiate bone modelling, which increases the ability of the bone to withstand further acute stressors. Whereas, less active children are not exposed to habitual strains and have less modelling, so are less able to withstand stressors, and may respond to acute strains with remodelling to make up for the lack of strength. This is one possible explanation. Further research is needed to fully understand the nature of secondary osteon initiation, formation, and growth.

BIBLIOGRAPHY

Agnew, A. M., Streeter, M. A., & Stout, S. D. (2007). Histomorphological aging of subadults: a test of Streeter's method on a medieval archaeological population. *American Journal of Physical Anthropology*, 44, 61.

Ahlqvist, J., & Damsten, O. (1969). A modification of Kerley's method for the microscopic determination of age in human bone. *Journal of forensic sciences*, 14(2), 205.

Anderson, H. C., & Morris, D. C. (1993). Mineralization. *Physiology and Pharmacology of Bone*, 107, 267-298.

Anderson and Andrews (2001). The Human Remains. In: Hicks and Hicks (eds.). *St Gregory's Priory, Northgate, Canterbury Excavations 1988-1991*. Canterbury: Canterbury Archaeological Trust.

Ascenzi, A., Benvenuti, A., & Bonucci, E. (1982). The tensile properties of single osteonic lamellae: technical problems and preliminary results. *Journal of Biomechanics*, 15(1), 29-37.

Balthazard, L., & Lebrun, R. (1911). Les canaux de Havers de l'os humain aux différents ages. *Ann Hyg Pub Med Lég*, 15, 144-152.

Bass, S., Pearce, G., Bradney, M., Hendrich, E., Delmas, P. D., Harding, A., & Seeman, E. (1998). Exercise before puberty may confer residual benefits in bone density in adulthood: studies in active prepubertal and retired female gymnasts. *Journal of Bone and Mineral Research*, 13(3), 500-507.

Bass, S. L., Saxon, L., Daly, R. M., Turner, C. H., Robling, A. G., Seeman, E., & Stuckey, S. (2002). The effect of mechanical loading on the size and shape of

bone in pre−, peri−, and postpubertal girls: a study in tennis players. *Journal of Bone and Mineral Research*, 17(12), 2274-2280.

Benjamin, M., & Ralphs, J. R. (1998). Fibrocartilage in tendons and ligaments—an adaptation to compressive load. *Journal of Anatomy*, 193(4), 481-494.

Benjamin, M., Kumai, T., Milz, S., Boszczyk, B. M., Boszczyk, A. A., & Ralphs, J. R. (2002). The skeletal attachment of tendons—tendon 'entheses'. *Comparative Biochemistry and Physiology Part A: Molecular & Integrative Physiology*, 133(4), 931-945.

Benjamin, M., & Hillen, B. (2003). Mechanical influences on cells, tissues and organs 'Mechanical Morphogenesis'. *European Journal of Morphology*, 41(1), 3-7.

Bloebaum, R. D., & Kopp, D. V. (2004). Remodeling capacity of calcified fibrocartilage of the hip. *The Anatomical Record Part A: Discoveries in Molecular, Cellular, and Evolutionary Biology*, 279(2), 736-739.

Boersma, B., & Wit, J. M. (1997). Catch-up growth. *Endocrine Reviews*, 18(5), 646-661.

Bowman, J. E., MacLaughlin, S. M., & Scheuer, J. L. (1992). The relationship between biological and chronological age in juvenile remains from St. Bride's Church, Fleet Street. *Annals of Human Biology*, 19, 216.

Brace, N., Kemp, R., and Snelgar, R. (2009). *SPSS for Psychologists*. Palgrave macmillan.

Bradbury, S., & Bracegirdle, B. (1998). *Introduction to light microscopy*. RMS Microscopy Handbooks, 42. Oxford, UK.: Bios Scientific publishers.

Bradney, M., Pearce, G., Naughton, G., Sullivan, C., Bass, S., Beck, T., & Seeman, E. (1998). Moderate exercise during growth in prepubertal boys: changes in bone mass, size, volumetric density, and bone strength: a controlled prospective study. *Journal of Bone and Mineral Research*, 13(12), 1814-1821.

Bright, R. W., & Elmore, S. M. (1968). Physical properties of epiphyseal plate cartilage. *In Surgical forum*, 19, 463.

Britz, H. M., Thomas, C. D., Clement, J. G., & Cooper, D. M. (2009). The relation of femoral osteon geometry to age, sex, height and weight. *Bone*, 45(1), 77-83.

Bruder, S. P., & Caplan, A. I. (1989). First bone formation and the dissection of an osteogenic lineage in the embryonic chick tibia is revealed by monoclonal antibodies against osteoblasts. *Bone*, 10(5), 359-375.

Buikstra, J. and Ubelaker, D. H. (1994). *Standards for Data Collection from Human Skeletal Remains*. Proceedings of a Seminar at the Field Museum of Natural History, Fayetteville: Arkansas Archaeological Survey Research Series, No. 44.

Burton, P., Nyssen-Behets, C., & Dhem, A. (1989). Haversian bone remodelling in human fetus. *Cells Tissues Organs*, 135(2), 171-175.

Caffey J (1993) *Pediatric X-ray diagnosis: an integrated imaging approach*. 9th edn. Mosby, St. Louis.

Cambra−Moo, O., Nacarino Meneses, C., Rodríguez Barbero, M. Á., García Gil, O., Rascón Pérez, J., Rello−Varona, S., & González Martín, A. (2014). An approach to the histomorphological and histochemical variations of the humerus cortical bone through human ontogeny. *Journal of Anatomy*, 224(6), 634-646.

Cardoso, H. F. (2005). Patterns of growth and development of the human skeleton and dentition in relation to environmental quality. Unpublished PhD thesis in Anthropology. McMaster University: Hamilton, Ontario.

Cardoso, H. F. (2007). Environmental effects on skeletal versus dental development: using a documented subadult skeletal sample to test a basic assumption in human osteological research. *American Journal of Physical Anthropology*, 132(2), 223-233.

Carter, D. R., & Beaupré, G. S. (2001). *Skeletal form and function: mechanobiology of skeletal development, aging and regeneration*. Cambridge: Press Syndicate of the University of Cambridge.

Castanet, J., Curry-Rogers, K., Cubo, J. and Boisard, J. J. (2000). Periosteal bone growth rates in extant ratites (ostriche and emu). Implications for assessing growth in Dinosaurs. *C.R. Acad. Sci. III Vie* 323, 43-550.

Cera, F., & Drusini, A. (1985). Analisi critica e sperimentale dei metodi di determinazione dell'eta attraverso le microstrutture ossee. *Quaderni di Anatomia Pratica*, 41, 105-121.

Chamay, A. (1970). Mechanical and morphological aspects of experimental overload and fatigue in bone. *Journal of Biomechanics*, 3(3), 263-270.

Cho, H., Stout, S. D., Madsen, R. W., & Streeter, M. A. (2002). Population-specific histological age-estimating method: a model for known African-American and European-American skeletal remains. *Journal of Forensic Sciences*, 47(1), 12-18.

Cho, H. (2012) In: Crowder, C., & Stout, S. (Eds.). *Bone histology: an anthropological perspective*. CRC Press.

Clover, V. H., & Gibson, M. T. (1979). *The letters of Lanfranc, archbishop of Canterbury*. Oxford University Press.

Cocchi, U. (1950). Polytope erbliche enchondrale Dysostosen. *RöFo-Fortschritte auf dem Gebiet der Röntgenstrahlen und der bildgebenden Verfahren*, 72(10), 409-435.

Cohn, I. (1924). Normal bones and joints. *Annals of Roentgenology*. New York City, iv.

Cool, S. M., Hendrikz, J. K., & Wood, W. B. (1995). Microscopic age changes in human occipital bone. *Journal of Forensic Science*, 40, 789-796.

Croft, M. A., Glasser, A., Heatley, G., McDonald, J., Ebbert, T., Dahl, D. B., & Kaufman, P. L. (2006). Accommodative ciliary body and lens function in rhesus monkeys, I: normal lens, zonule and ciliary process configuration in the iridectomized eye. *Investigative Ophthalmology and Visual Science*, 47(3), 1076.

Crowder, C., & Stout, S. (Eds.). (2012). *Bone histology: an anthropological perspective*. CRC Press.

Cubo, J., Legendre, P., De Ricqlès, A., Montes, L., De Margerie, E., Castanet, J., & Desdevises, Y. (2008). Phylogenetic, functional, and structural components of variation in bone growth rate of amniotes. *Evolution & development*, 10(2), 217-227.

Currey, J. D. (1964). Some effects of ageing in human Haversian systems. *Journal of Anatomy*, 98(1), 69.

Currey, J. D. (1984). *The Mechanical Adaptations of Bones*. Princeton, NJ: Princeton University.

Currey, J. D. (2002). *Bones: structure and mechanics*. Princeton University Press.

Davies, D. A., & Parsons, F. G. (1927). The age order of the appearance and union of the normal epiphyses as seen by X-rays. *Journal of Anatomy*, 62(1), 58.

de Boer, H. H., Aarents, M. J., & Maat, G. J. R. (2012). Staining ground sections of natural dry bone tissue for microscopy. *International Journal of Osteoarchaeology*, 22, 379-386.

Demirjian, A. (1986). Dentition. In: *Postnatal Growth Neurobiology*, pp. 269-298. Springer US.

Dertina, D., Loro, M. L., Sayre, J., Kaufman, F., & Gilsanz, V. (1998). Childhood bone measurements predict values at young adulthood. *Bone*, 23(1), 288.

Dodd JS, Raleigh JA, Gross TS. 1999. Osteocyte hypoxia: a novel mechanotransduction pathway. *American Journal of Physiology*, 277(1), 598-602.

Drusini, A., & Businaro, F. (1990). Skeletal age determination by mandibular histomorphometry. *International Journal of Anthropology*, 5(3), 235-243.

Elgenmark, O. (1946). Preface. *Acta Paediatrica*, 33(1), 7-8.

Enlow, D. H. (1963). *Principles of bone remodeling*.

Ericksen, M. F. (1976). Cortical bone loss with age in three Native American populations. *American Journal of Physical Anthropology*. 45, 443-452.

Ericksen, M. F. (1991). Histologic estimation of age at death using the anterior cortex of the femur. *American Journal of Physical Anthropology*, 84(2), 171-179.

Everts, V., Delaisse, J. M., Korper, W., Jansen, D. C., Tigchelaar−Gutter, W., Saftig, P., & Beertsen, W. (2002). The bone lining cell: its role in cleaning Howship's

lacunae and initiating bone formation. *Journal of Bone and Mineral Research*, 17(1), 77-90.

Fangwu, Z. (1983). Preliminary study on determination of bone age by microscopic method. *Acta Anthropologica Sinica*, 2, 142-151.

Ferrari, S., Rizzoli, R., Slosman, D., & Bonjour, J. P. (1998). Familial resemblance for bone mineral Mass is Expressed before Puberty 1. *The Journal of Clinical Endocrinology & Metabolism*, 83(2), 358-361.

Fraser, J. R. E., Laurent, T. C., & Laurent, U. B. G. (1997). Hyaluronan: its nature, distribution, functions and turnover. *Journal of Internal Medicine*, 242(1), 27-33.

Frost, H. M. (1986). Bone microdamage: factors that impair its repair. In: *Current concepts of bone fragility* (pp. 123-146). Springer Berlin Heidelberg.

Frost, H. M. (1987). Bone “mass” and the “mechanostat”: a proposal. *The anatomical Record*, 219(1), 1-9.

Frost, H. M. (1990). Skeletal structural adaptations to mechanical usage (SATMU): 1. Redefining Wolff's law: the bone modeling problem. *The Anatomical Record*, 226(4), 403-413.

Frost, H. M. (1997). Why do long-distance runners not have more bone? A vital biomechanical explanation and an estrogen effect. *Journal of Bone and Mineral Metabolism*, 15(1), 9-16.

Fujimura R., Noriko A., Watanabe M., Mukai N., Amagai H., Fuku- bayashi T., Hayashi K., Tokuyama K., Suzuki M. (1997). Effect of resistance exercise training on bone formation and resorption in young male subjects assessed by biomarkers of bone metabolism. *Journal of Bone and Mineral Research*, 12, 656–662.

Garn, S. M. Rohmann, C. G., Blumenthal, T., & Silverman, F. N. (1967). Ossification communalities of the hand and other body parts: Their implication to skeletal assessment. *American Journal of Physical Anthropology*, 27(1), 75-82.

Garn, S. M. (1970). *The earlier gain and the later loss of cortical bone, in nutritional perspective*. Springfield, Illinois, USA.

Glenister, T. W. (1976). An embryological view of cartilage. *Journal of Anatomy*, 122(2), 323.

Goldman, H. M., Mcfarlin, S. C., Cooper, D. M., Thomas, C. D. L., & Clement, J. G. (2009). Ontogenetic Patterning of Cortical Bone Microstructure and Geometry at the Human Mid−Shaft Femur. *The Anatomical Record*, 292(1), 48-64.

Goodship, A. E., & Cunningham, J. L. (2001). *Pathophysiology of functional adaptation of bone in remodelling and repair in-vivo*.

Gosman, J. H., Hubbell, Z. R., Shaw, C. N., & Ryan, T. M. (2013). Development of cortical bone geometry in the human femoral and tibial diaphysis. *The Anatomical Record*, 296(5), 774-787.

Gray, H. (2012). Gray's Anatomy. 15th edition. London: Bounty Books.

Haines, R. W., Mohiuddin, A., Okpa, F. I., & Viega-Pires, J. A. (1967). The sites of early epiphysial union in the limb girdles and major long bones of man. *Journal of Anatomy*, 101(Pt 4), 823.

Hamilton, W. J., Mossman, H. W., & Boyd, J. D. (1972). *Human Embryology: Prenetal Development of Form and Function*. Williams & Wilkins.

Han, S. H., Kim, S. H., Ahn, Y. W., Huh, G. Y., Kwak, D. S., Park, D. K., & Kim, Y. S. (2009). Microscopic Age Estimation from the Anterior Cortex of the Femur in Korean Adults. *Journal of Forensic Sciences*, 54(3), 519-522.

Hansman, C. F. (1962). Appearance and fusion of ossification centers in the human skeleton. *The American Journal of Roentgenology*, 88, 476-482.

Haraldsson, S. (1959). On osteochondrosis deformans juvenilis capituli humeri including the investigation of intra-osseous vasculature in distal humerus. *Acta Orthopaedica*, 30(38), 5-232.

Hauser, R., Barres, D., Durigon, M., & Derobert, L. (1980). Identification using histomorphometry of the femur and tibia. *Acta Medicinae Legalis et Socialis*, 30(2), 91.

Heaney, R. P., Abrams, S., Dawson-Hughes, B., Looker, A., Looker, A., Marcus, R., & Weaver, C. (2000). Peak Bone Mass. *Osteoporosis International*, 11(12), 985-1009.

Hennig, C., Thomas, C. D. L., Clement, J. G., & Cooper, D. M. (2015). Does 3D orientation account for variation in osteon morphology assessed by 2D histology?. *Journal of Anatomy*.

Hicks, M., and Hicks, A. (2001). *St. Gregory's Priory, Northgate, Canterbury Excavations 1988-1989*. Canterbury Archaeological Trust Ltd.

Hoppa, R. D. (1992). Evaluating human skeletal growth: An Anglo−Saxon example. *International Journal of Osteoarchaeology*, 2(4), 275-288.

Johnson, L. C. (1964). Morphologic analysis in pathology: the kinetics of disease and general biology of bone. *Bone Biodynamics*, 1, 543-654.

Kerley, E. R. (1965). The microscopic determination of age in human bone. *American Journal of Physical Anthropology*, 23(2), 149-163.

Kerley, E. R., & Ubelaker, D. H. (1978). Revisions in the microscopic method of estimating age at death in human cortical bone. *American Journal of Physical Anthropology*, 49(4), 545-546.

Kimura, K. (1992). Estimation of age at death from second metacarpals. *Zeitschrift für Morphologie und Anthropologie*, 79, 169-181.

Knudson, C. B., & Toole, B. P. (1987). Hyaluronate-cell interactions during differentiation of chick embryo limb mesoderm. *Developmental Biology*, 124(1), 82-90.

Lewis, A. B., & Garn, S. M. (1960). The relationship between tooth formation and other maturational factors. *The Angle Orthodontist*, 30(2), 70-77.

Lieberman, D. E., & Crompton, A. W. (1998). Responses of bone to stress. *Principles of Biological Design: The Optimization and Symmorphosis Debate*, 78-86.

Lieberman, D. E., Devlin, M., & Pearson, O. (2001). Articular area responses to mechanical loading: effects of exercise, age and skeletal location. *American Journal of Physical Anthropology*, 116, 266–277.

Lieberman, D. E., Pearson, O. M., Polk, J. D., Demes, B., & Crompton, A. W. (2003). Optimization of bone growth and remodeling in response to loading in tapered mammalian limbs. *Journal of Experimental Biology*, 206(18), 3125-3138.

Lovejoy, C. O., Meindl, R. S., Mensforth, R. P., & Barton, T. J. (1985). Multifactorial determination of skeletal age at death: a method and blind tests of its accuracy. *American Journal of Physical Anthropology*, 68(1), 1-14.

Maggiano, I. S., Maggiano, C. M., Tiesler, V., Kierdorf, H., Stout, S. D., & Schultz, M. (2011). A distinct region of microarchitectural variation in femoral compact bone: histomorphology of the endosteal lamellar pocket. *International Journal of Osteoarchaeology*, 21(6), 743-750.

Maresh, M. M., & Beal, V. A. (1970). A longitudinal survey of nutrition intake, body size, and tissue measurements in healthy subjects during growth. *Monographs of the Society for Research in Child Development*, 33-39.

Marks, S. C., & Odgren, P. R. (2002). Structure and development of the skeleton. In: J. P. Bilezikian, L. G. Raisz, & G. A. Rodan (Eds.), *Principles of bone biology* (Vol. 1, pp. 3–15). San Diego: Academic Press.

Marsh R. L., Ellerby D. J., Carr J. A., Henry H. T., & Buchanan C. I. (2004). Partitioning the energetics of walking and running: swinging the limbs is expensive. *Science*, 303, 80–83.

Martin, R. B., & Burr, D. B. (1989). *Structure, function, and adaptation of compact bone*. Raven Press.

Martin R. B. (1995). A mathematical model for fatigue damage repair and stress fracture in osteonal bone. *Journal of Orthopaedic Research*, 13, 309 –316.

Martin, R. B., Burr, D. B., & Sharkey, N. A. (1998). *Skeletal Tissue Mechanics*. Springer.

Martin, R. B. (2000). Toward a unifying theory of bone remodeling. *Bone*, 26(1), 1-6.

Martiniaková, M., Omelka, R., Chrenek, P., Ryban, L., Parkányi, V., Grosskopf, B., & Bauerová, M. (2005). Changes of femoral bone tissue microstructure in transgenic rabbits. *Folia Biologica Praha*, 51(5), 140.

Martrille, L., Irinopoulou, T., Bruneval, P., Baccino, E., & Fornes, P. (2009). Age at Death Estimation in Adults by Computer−Assisted Histomorphometry of Decalcified Femur Cortex. *Journal of Forensic Sciences*, 54(6), 1231-1237.

Mays, S. (2008). Septal aperture of the humerus in a mediaeval human skeletal population. *American Journal of Physical Anthropology*, 136(4), 432-440.

McFarlin, S. C. (2006). *Ontogenetic variation in long bone microstructure in catarrhines and its significance for life history research*. ProQuest.

McKern, T. W., & Stewart, T. D. (1957). Skeletal age changes in young american males. *Headquarters, Quartermaster Research and Development Command*. Technical Report EP-45.

Menees, T. O., & Holly, L. E. (1932). The ossification in the extremities of the newborn. *American Journal Roentgenology*, 28, 389-390.

Miszkiewicz, J. J. (2012). Linear enamel hypoplasia and age-at-death at Medieval (11th–16th Centuries) St. Gregory's Priory and Cemetery, Canterbury, UK. *International Journal of Osteoarchaeology*, 25(1), 79-87.

Miszkiewicz, J. J. (2015). Investigating histomorphometric relationships at the human femoral midshaft in a biomechanical context. Journal of Bone and Mineral Metabolism, 1-14.

Moorrees, C. F., Fanning, E. A., & Hunt Jr, E. E. (1963). Age variation of formation stages for ten permanent teeth. *Journal of Dental Research*, 42(6), 1490-1502.

Murphy, D. B. (2001). *Fundamentals of light microscopy and electronic equipment*. Wiley-Liss, New York.

Narasaki, S. (1990). Estimation of age at death by femoral osteon remodeling: application of Thompson's core technique to modern Japanese. *Journal of the Anthropological Society of Nippon*, 98, 29-38.

Ogden, J. A., Conlogue, G. J., & Jensen, P. (1978). Radiology of postnatal skeletal development: the proximal humerus. *Skeletal Radiology*, 2(3), 153-160.

Ogden, J. A., Conlogue, G. J., & Bronson, M. L. (1979). Radiology of postnatal skeletal development. *Skeletal Radiology*, 4(4), 196-203.

Ogden, J. A. (1984). Radiology of postnatal skeletal development. *Skeletal Radiology*, 12(3), 169-177.

O'Rahilly, R., Gardner, E., & Gray, D. J. (1956). The ectodermal thickening and ridge in the limbs of staged human embryos. *Journal of Embryology and Experimental Morphology*, 4(3), 254-264.

O'Rahilly, R., & Gardner, E. (1975). The timing and sequence of events in the development of the limbs in the human embryo. *Anatomy and Embryology*, 148(1), 1-23.

Ozonoff, M. B. (1979). *Pediatric orthopedic radiology* (Vol. 15). Saunders Limited.

Parfitt, A. M. (2002). Targeted and nontargeted bone remodeling: relationship to basic multicellular unit origination and progression. *Bone*, 30(1), 5-7.

Paterson, R. S. (1929). A radiological investigation of the epiphyses of the long bones. *Journal of Anatomy*, 64(1), 28.

Pearson, O. M. (2000). Activity, climate, and postcranial robusticity. *Current Anthropology*, 41(4), 569-607.

Pearson, O. M., & Lieberman, D. E. (2004). The aging of Wolff's "law": ontogeny and responses to mechanical loading in cortical bone. *American Journal of Physical Anthropology*, 125(39), 63-99.

Pfeiffer, S., Crowder, C., Harrington, L., & Brown, M. (2006). Secondary osteon and Haversian canal dimensions as behavioral indicators. *American Journal of Physical Anthropology*, 131(4), 460-468.

Pritchett, J. W. (1991). Growth plate activity in the upper extremity. *Clinical Orthopaedics and Related Research*, 268, 235-242.

Qiu, S., Fyhrie, D. P., Palnitkar, S., & Rao, D. S. (2003). Histomorphometric assessment of Haversian canal and osteocyte lacunae in different−sized osteons in human rib. *The Anatomical Record Part A: Discoveries in Molecular, Cellular, and Evolutionary Biology*, 272(2), 520-525.

Rang, M. (1969). The growth plate and its disorders. In; *The growth plate and its disorders*. E. & S. Livingstone Ltd.

Robey, P. G., & Boskey, A. L. (2009). The composition of bone. *Primer on the Metabolic Bone Diseases and Disorders of Mineral Metabolism*, 7, 32-38.

Robling, A. G., Castillo, A. B., & Turner, C. H. (2006). Biomechanical and molecular regulation of bone remodeling. *Annual Review of Biomedical Engineering*, 8, 455-498.

Robling, A. G., & Stout, S. D. (1999). Morphology of the drifting osteon. *Cells Tissues Organs*, 164(4), 192-204.

Robling, A. G., & Stout, S. D. (2008). Histomorphometry of human cortical bone: applications of age estimation. In: MA Katzenberg & SR Saunders, (eds).

Biological Anthropology of the Human Skeleton, pp. 148-182. John Wiley & Sons.

Rother, P., Krüger, G., Machlitt, J., & Hunger, H. (1978). Investigations on the aging processes of the humerus by means of histomorphometry, regression and factor analysis. *Anatomischer Anzeiger*, 144(4), 346-365.

Ruff, C. B., Walker, A., & Trinkaus, E. (1994). Postcranial robusticity in Homo. III: ontogeny. *American Journal of Physical Anthropology*, 93(1), 35-54.

Ruff, C. B. (2000). Body size, body shape, and long bone strength in modern humans. *Journal of Human Evolution*, 38(2), 269-290. John Wiley & Sons.

Ruff, C. B. (2007). Biomechanical analyses of archaeological human skeletons. In: MA Katzenberg & SR Saunders, (eds). *Biological Anthropology of the Human Skeleton*, Second Edition, pp. 183-206.

Samson, C., & Branigan, K. (1987). A new method of estimating age at death from fragmentary and weathered bone. *Death, Decay and Reconstruction. Approaches to Archaeology and Forensic Science*, Manchester University Press, Manchester, 101-108.

Saunders, S. R., & Hoppa, R. D. (1993). Growth deficit in survivors and non−survivors: Biological mortality bias in subadult skeletal samples. *American Journal of Physical Anthropology*, 36(17), 127-151.

Schaffler, M. B., Radin, E. L., & Burr, D. B. (1990). Long-term fatigue behavior of compact bone at low strain magnitude and rate. *Bone*, 11(5), 321-326.

Scheuer, L., & Black, S. (2000). *Developmental Juvenile Osteology*. Academic Press.

Schillaci, M. A., Nikitovic, D., Akins, N. J., Tripp, L., & Palkovich, A. M. (2011). Infant and juvenile growth in ancestral Pueblo Indians. *American Journal of Physical Anthropology*, 145(2), 318-326.

Schlecht, S. (2012). Understanding Entheses: Bridging the Gap Between Clinical and Anthropological Perspectives. *The Anatomical Record*, 295, 1239-1251.

Sherwood, R. J., Meindl, R. S., Robinson, H. B., and May, R. L. (2000). Fetal age: Methods of estimation and effects of pathology. *American Journal of Physical Anthropology*, 113, 305-316.

Shopfner, C. E. (1966). Periosteal bone growth in normal infants: a preliminary report. *American Journal of Roentgenology*, 97(1), 154-163.

Silberstein, M. J., Brodeur, A. E., & Graviss, E. R. (1979). Some vagaries of the capitellum. *The Journal of Bone and Joint Surgery*, 61(2), 244-247.

Silberstein, M. J., Brodeur, A. E., Graviss, E. R., & Luisiri, A. T. (1981). Some vagaries of the medial epicondyle. *The Journal of Bone and Joint Surgery*, 63(4), 524-528.

Silberstein, M. J., Brodeur, A. E., & Graviss, E. R. (1982). Some vagaries of the lateral epicondyle. *The Journal of Bone and Joint Surgery*, 64(3), 444-448.

Singh, I. J., & Gunberg, D. L. (1970). Estimation of age at detain human males from quantitative histology of bone fragments. *American Journal of Physical Anthropology*, 33, 373-382.

Skawina, A., Mazurkiewicz, S., Litak, A., & Wyczółkowski, M. (1987). Cortico-diaphyseal indicators in the evaluation of the mechanical strength of the second metacarpal bone. *Chirurgia Narzadów Ruchu i Ortopedia Polska*, 52(2), 108.

Skedros, J. G., Mason, M. W., & Bloebaum, R. D. (1994). Differences in osteonal micromorphology between tensile and compressive cortices of a bending skeletal system: indications of potential strain-specific differences in bone microstructure. *Anatomical Record*, 239, 405–413.

Skedros, J. G., Holmes, J. L., Vajda, E. G., & Bloebaum, R. D. (2005). Cement lines of secondary osteons in human bone are not mineral−deficient: New data in a historical perspective. *The Anatomical Record Part A: Discoveries in Molecular, Cellular, and Evolutionary Biology*, 286(1), 781-803.

Slack, J. M. W. (2013). *Essential Developmental Biology*, Third edition. Wiley-Blackwell.

Slayter, E. M., & Slayter, H. S. (1992). *Light and electron microscopy*. Cambridge University Press.

Smith, B. H., & Garn, S. M. (1987). *Polymorphisms in eruption sequence of permanent teeth in American children*.

Smith, B. H. (1991). Dental development and the evolution of life history in Hominidae. *American Journal of Physical Anthropology*, 86(2), 157-174.

Smith, R. F. (1994). *Microscopy and photomicrography: a working manual*, 2 edn. CRC Press, Boca Raton, Florida.

Spencer, H. R. (1891). Ossification in the head of the humerus at birth. *Journal of Anatomy and Physiology*, 25(Pt 4), 552.

Starck, J. M., & Chinsamy, A. (2002). Bone microstructure and developmental plasticity in birds and other dinosaurs. *Journal of Morphology*, 254(3), 232-246.

Stock, J. T., & Shaw, C. N. (2007). Which measures of diaphyseal robusticity are robust? A comparison of external methods of quantifying the strength of long bone diaphyses to cross-sectional geometric properties. *American Journal of Physical Anthropology*, 134(3), 412.

Stout, S. D., & Paine, R. R. (1992). Histological age estimation using rib and clavicle. *American Journal of Physical Anthropology*, 87(1), 111-115.

Stout, S. D., & Lueck, R. (1995). Bone remodeling rates and skeletal maturation in three archaeological skeletal populations. *American Journal of Physical Anthropology*, 98(2), 161-171.

Stout, S. & Crowder, C. (2012) In: Crowder, C., & Stout, S. (Eds.). *Bone histology: an anthropological perspective*. CRC Press.

Streeter, M. (2005). Histomorphometric characteristics of the subadult rib cortex: normal patterns of dynamicc bone modeling and remodeling during growth and development. Dissertation, University of Missouri, Columbia.

Streeter, M., & Stout, S. D. (2006). Age estimation method for the subadult rib cortex. *American Journal of Physical Anthropology*. 173-173.

Streeter, M. (2012). The determination of age in subadult from the rib cortical microstructure. In: Bell, L. S. (ed). *Forensic Microscopy for Skeletal Tissues: Methods and Protocols*. Humana Press: New York.

Tatton-Brown T. 1995. The beginnings of St. Gregory's Priory and St. John's Hospital in Canterbury. In: Eales, R., Sharpe, R. (eds). *Canterbury and the Norman Conquest: Churches, saints and scholars 1066-1109*. London: The Hambledon Press. p. 41 – 52.

Thomopoulos, S., Das, R., Birman, V., Smith, L., Ku, K., Elson, E. L., & Genin, G. M. (2011). Fibrocartilage tissue engineering: the role of the stress environment on cell morphology and matrix expression. *Tissue Engineering Part A*, 17(7-8), 1039-1053.

Thompson, D. D. (1979). The core technique in the determination of age at death in skeletons. *Journal of Forensic Science*, 24(4), 902-915.

Thompson, D. D., & Galvin, C. A. (1983). Estimation of age at death by tibial osteon remodeling in an autopsy series. *Forensic Science International*, 22(2), 203-211.

Trinkaus, E. (1983). Neandertal postcrania and the adaptive shift to modern humans. *The Mousterian Legacy: Human Biocultural Adaptations in the Later Pleistocene, British Archaeological Reports International Series*, Oxford, UK, 165-200.

Tsonis, P. A. (2008). Stem cells and blastema cells. *Current Stem Cell Research and Therapy*, 3(1), 53-54.

Ubelaker, D. H. (1987). Estimating age at death from immature human skeletons: an overview. *Journal of Forensic Sciences*, 32(5), 1254-1263.

Ubelaker, D. H. (1989). The estimation of age at death from immature human bone. *Age Markers in the Human Skeleton*, 55-70.

Uytterschaut, H. T. (1985). Determination of skeletal age by histological methods. *Zeitschrift für Morphologie und Anthropologie*, 331-340.

van Oers, R. F., Ruimerman, R., Tanck, E., Hilbers, P. A., & Huiskes, R. (2008). A unified theory for osteonal and hemi-osteonal remodeling. *Bone*, 42(2), 250-259.

Villa, C., & Lynnerup, N. (2010). Technical note: A stereological analysis of the cross‐sectional variability of the femoral osteon population. *American Journal of Physical Anthropology*, 142(3), 491-496.

Watanabee, Y., Konishi, M., Shimada, M., Ohara, H., & Iwamoto, S. (1998). Estimation of age from the femur of Japanese cadavers. *Forensic Science International*, 98, 55-65.

Weinmann, J. P., & Sicher, H. (1947). Bone and Bones, CV Mosby Co. St. Louis.

White, T. D., Black, M. T., & Folkens, P. A. (2011). *Human osteology*. Academic press.

Wolff, J. (1892). Das gesetz der transformation der knochen. *DMW-Deutsche Medizinische Wochenschrift*, 19(47), 1222-1224.

Yoshino, M., Imaizuni, K., Miyasaka, S., & Seta, S. (1994). Histological estimation of age at death using microradiographs of humeral compact bone. *Forensic Science International*, 64, 191-198.

APPENDIX 1
ANOVA RESULTS

Age Classes

Variables	dF	F	p
Height	3,54	132.479	0.000
Robusticy index	3,75	12.608	0.000
Osteon population density	3,79	12.207	0.000
Primary osteon population density	3,79	27.945	0.000
Secondary osteon population density	3,79	103.152	0.000
Primary canal area	3,72	1.009	0.394
Primary canal minimum diameter	3,72	2.555	0.062
Primary canal maximum diameter	3,72	1.168	0.328
Secondary osteon area	2,61	4.676	0.013
Secondary osteon minimum diameter	2,60	1.303	0.279
Secondary osteon maximum diameter	2,60	13.571	0.000
Secondary canal area	2,61	0.380	0.686
Secondary canal minimum diameter	2,60	8.725	0.000
Secondary canal maximum diameter	2,60	7.286	0.001
Number of lacunae	2,19	1.934	0.172

Robusticity Groups

Variables	dF	F	p
Height	2,28	7.361	0.003
Osteon population density	2,32	2.892	0.070
Primary osteon population density	2,32	0.304	0.740
Secondary osteon population density	2,32	12.732	0.000
Primary canal area	2,32	0.947	0.398
Primary canal minimum diameter	2,32	0.772	0.471
Primary canal maximum diameter	2,32	4.180	0.064
Secondary osteon area	2,19	2.284	0.129
Secondary osteon minimum diameter	2,18	1.056	0.368
Secondary osteon maximum diameter	2,18	2.458	0.114
Secondary canal area	2,19	0.603	0.558
Secondary canal minimum diameter	2,18	0.107	0.899
Secondary canal maximum diameter	2,18	0.924	0.415
Number of lacunae	2,4	0.579	0.601

APPENDIX 2
PEARSON'S RESULTS

Age Classes

	Rs	N	p
Height	0.945	73	0.000
Robusticy index	-0.660	79	0.000
Osteon population density	0.514	83	0.000
Primary osteon population density	-0.672	83	0.000
Secondary osteon population density	0.878	79	0.000
Primary canal area	-0.012	76	0.915
Primary canal minimum diameter	0.072	76	0.538
Primary canal maximum diameter	-0.196	76	0.090
Secondary osteon area	0.392	64	0.001
Secondary osteon minimum diameter	-0.149	63	0.244
Secondary osteon maximum diameter	0.559	63	0.000
Secondary canal area	-0.031	64	0.808
Secondary canal minimum diameter	-0.475	63	0.000
Secondary canal maximum diameter	0.439	63	0.000
Number of lacunae	-0.392	22	0.071

Robusticity Groups

	Rs	N	p
Height	-0.523	31	0.003
Osteon population density	-0.379	35	0.025
Primary osteon population density	0.050	35	0.777
Secondary osteon population density	-0.642	35	0.000
Primary canal area	-0.162	35	0.353
Primary canal minimum diameter	0.162	35	0.354
Primary canal maximum diameter	-0.351	35	0.038
Secondary osteon area	-0.398	22	0.067
Secondary osteon minimum diameter	-0.193	21	0.401
Secondary osteon maximum diameter	-0.462	21	0.035
Secondary canal area	-0.084	22	0.711
Secondary canal minimum diameter	-0.090	21	0.697
Secondary canal maximum diameter	-0.213	21	0.354
Number of lacunae	-0.578	7	0.174